A stochastic gradient descent method for computational design of random rough surfaces in solar cells

Qiang Li[1,*], Gang Bao[2], Yanzhao Cao[3] and Junshan Lin[3]

[1] *Institute of Computational Mathematics and Scientific/Engineering Computing, Academy of Mathematics and Systems Science, Chinese Academy of Sciences, Beijing 100190, China.*
[2] *Department of Mathematics, Zhejiang University, China.*
[3] *Department of Mathematics and Statistics, Auburn University, Auburn, AL 36849, USA.*

Abstract. In this work, we develop a stochastic gradient descent method for the computational optimal design of random rough surfaces in thin-film solar cells. We formulate the design problems as random PDE-constrained optimization problems and seek the optimal statistical parameters for the random surfaces. The optimizations at fixed frequency as well as at multiple frequencies and multiple incident angles are investigated. To evaluate the gradient of the objective function, we derive the shape derivatives for the interfaces and apply the adjoint state method to perform the computation. The stochastic gradient descent method evaluates the gradient of the objective function only at a few samples for each iteration, which reduces the computational cost significantly. Various numerical experiments are conducted to illustrate the efficiency of the method and significant increases of the absorptance for the optimal random structures. We also examine the convergence of the stochastic gradient descent algorithm theoretically and prove that the numerical method is convergent under certain assumptions for the random interfaces.

AMS subject classifications: 35J05, 35Q60, 49M41, 49Q10, 65C05, 65C30, 60H35

Key words: Optimal design, random rough surface, solar cell, Helmholtz equation, stochastic gradient descent method.

1 Introduction

Thin-film silicon solar cell is an attractive photovoltaic device because it attains a small thickness, which results in significant savings of material and energy during the fabrication. The cell consists of hydrogenated amorphous silicon (a-Si:H) as the absorbing layer,

*Corresponding author. *Email addresses:* liqiang@amss.ac.cn (Q. Li), bao@math.zju.edu.cn (G. Bao), yzc0009@auburn.edul (Y. Cao), jzl0097@auburn.edu (J. Lin).

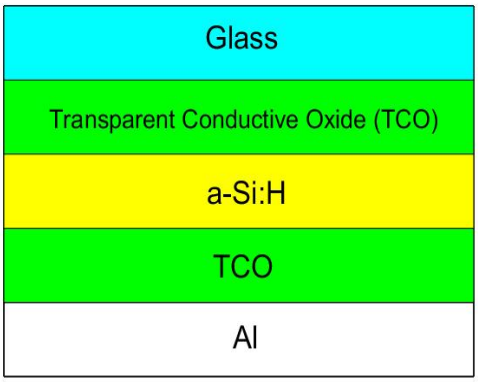

Figure 1: A schematic plot of thin-film solar cells.

sandwiched between the transparent conductive oxide (TCO) layers for conducting the electric current. Figure 1 shows the structure of a typical thin-film solar cell, wherein the glass substrate on the top allows the incoming light to enter the cell and the highly reflective aluminum contact layer at the bottom enhances the absorption of light within the cell.

The a-Si:H layer in the thin-film solar cell is sufficiently absorptive at smaller optical wavelengths but poorly absorptive at larger wavelengths (typically >600 nm), which is responsible for the low overall efficiency of the cell. One way to increase the absorption within the solar cell and enhance its performance is to engineer the structure by texturing the interfaces between the different layers in a random manner [1, 10, 11, 13, 18, 22]. The randomly textured surfaces lower the reflection losses at the entrance facet and scatter the light, thereby increasing the optical path of each photon in the solar cell. In realistic fabrication, the surfaces of the TCO layers in Figure 1 are textured randomly, which is achieved at low cost by controlling the deposition parameter of TCO films sputtered on substrates [16]. We would also like to point out several other ways to increase the absorption efficiency of solar cells, such as anti-reflection coating, dielectric gratings, and plasmonic nanoparticles [3, 6, 9, 12, 19], although these techniques may be costly in fabrication.

The design and optimization of random surfaces in thin-film solar cells are mostly performed by the ad hoc procedures, where one computes the absorptance of the cell for chosen statistical parameters and obtains the optimal parameters from the comparison of the computed absorptance values [10, 11, 13, 18]. Such ad hoc schemes are computationally inefficient and the optimal solutions heavily depend on the set of statistical parameters being chosen. To provide a systematic computational framework, in [4] we formulate the optimal design of random surface textures as a random PDE-constrained problem and apply the gradient-based algorithm to solve the optimization problem. The optimization problem seeks to maximize the mean absorptance function for the solar cells by sampling random surfaces in the appropriate probability space. We employ the Monte-Carlo method for sampling the probability space in [4] and apply the adjoint state method for computing the gradient at each sample. The optimal random textures give

rises to significant absorption enhancement, with the photon absorptance much higher than the existing random textures.

Albeit being able to provide optimal random surface textures, the numerical algorithm based on the Monte-Carlo sampling and the adjoint state method is computationally expensive, due to the largeness of the samples needed in computing the gradient average and the necessity to solve the underlying governing PDEs to obtain the gradient for each sample. In this work, we adopt the stochastic gradient descent method, which is a key ingredient of machine learning algorithms (cf. [7]), to solve the stochastic optimization problems. The new algorithm can obtain the statistical parameters of the optimal random textures, and its computational cost is significantly lower compared to the full gradient descent approach. We show that the numerical method is convergent under certain assumptions on the step sizes of the iterative algorithm and the random interfaces. In addition, in contrast to the optimization of one single random interface in [4], we consider the optimization of several random interfaces as well as the optimization of the random boundary for the solar cell. We also investigate more sophisticated configurations when optimization is performed over a frequency band or with multiple incident angles, which are computationally formidable if one attempts to solve by the full gradient method developed in [4].

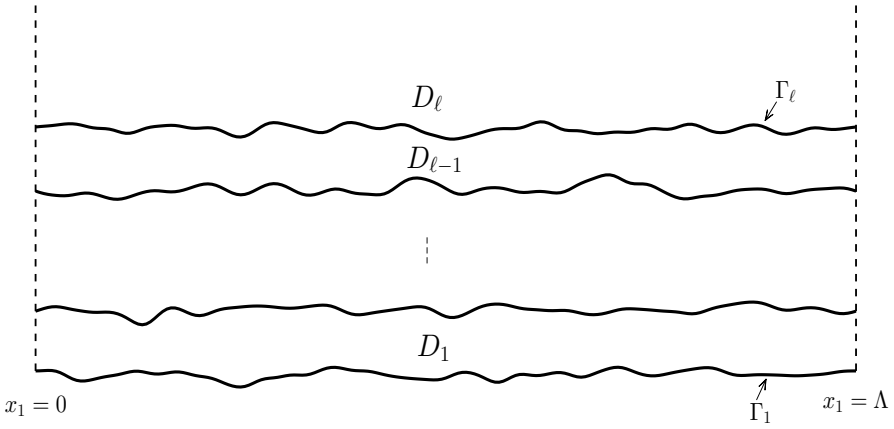

Figure 2: Schematic plot of the multi-layered medium in the reference periodic cell with $0 < x_1 < \Lambda$. The layers from the bottom to the top are $D_1, D_2, \cdots, D_\ell$. The boundary at the bottom is given by Γ_1 and the interface between the two layers D_{j-1} and D_j is given by Γ_j $(j = 2, \cdots, \ell)$.

More specifically, we consider the multi-layered structure in $\mathbb{R}^2$ as depicted in Figure 2, which consists of several layers $D_1, D_2, \cdots, D_\ell$ from the bottom to the top. The boundary at the bottom of the structure Γ_1 and the interface Γ_j $(j = 2, \cdots, \ell)$ between the two layers D_{j-1} and D_j are textured randomly. For each random sample ζ, the interface Γ_j is represented as $\Gamma_j(\zeta) := \{(x_1, x_2) \mid x_2 = f_j(\zeta, \alpha_j; x_1)\}$, wherein $\alpha_j \in \mathbb{R}^d$ represents the sta-

tistical parameters of the interface and f_j is the profile function for the interface. The optimization problem is to solve for the optimal statistical parameters $\{\alpha_j\}_{j=1}^{\ell}$ such that the overall absorbtance within these layers is maximized. The problem setup will be discussed in more details in Section 2.

The rest of the paper is organized as follows. In Section 2 we introduce the mathematical model for the optical scattering problem by random rough surfaces and formulate the optimal design problems. The shape derivatives and the gradient of the objective function are derived by the adjoint state method in Section 3. We present the stochastic gradient descent method for the optimization problems and examine the convergence of the method in Section 4. Finally, various numerical experiments are given in Section 5 to demonstrate the efficiency of the numerical method.

2 Mathematical formulation of the optimal design problems

2.1 Mathematical model for optical scattering problem by random surfaces

We assume that the whole structure is periodic along the x_1 direction with the period Λ, considering that the solar cells are usually arranged periodically in fabrication. For each random sample ζ and for $j=1,2,\cdots,\ell-1$, we let

$$D_j(\zeta) := \{(x_1,x_2) : 0 < x_1 < \Lambda_1, f_j(\zeta;x_1) < x_2 < f_{j+1}(\zeta;x_1)\} \tag{2.1}$$

be the jth layer in the reference period shown in Figure 2, and

$$D_\ell(\zeta) := \{(x_1,x_2) : 0 < x_1 < \Lambda_1, x_2 > f_\ell(\zeta;x_1)\} \tag{2.2}$$

be the domain on the top. For each j, the interface profile function satisfies

$$f_j(\zeta;x_1+\Lambda) = f_j(\zeta,x_1) \quad \text{for } -\infty < x_1 < \infty,$$

and $f_j(\zeta;x_1)$ is a stationary random process in the reference period with $0 < x_1 < \Lambda$. This will be elaborated in Section 2.2 .

The relative permittivity function ε_r attains the value $\varepsilon_{r,j}$ in each layer D_j. We consider the transverse electric (TE) polarization for the optical wave, in which the electric field attains the form $E = (0,0,u)$. The structure is illuminated by a time-harmonic incident plane wave $u^i = e^{ik_0 q_\ell (\sin\theta, -\cos\theta)\cdot x}$, where k_0 be the free-space wavenumber, $\theta \in (-\frac{\pi}{2}, \frac{\pi}{2})$ is the incident angle and $q_\ell := \sqrt{\varepsilon_{r,\ell}}$ represents the refractive index in D_ℓ. For simplicity of notation, here and henceforth, we set the wavenumber in D_ℓ as $k_\ell = k_0 q_\ell$ and express the incident wave as $u^i = e^{i(\tau x_1 - \rho x_2)}$, in which $\tau = k_\ell \sin\theta$ and $\rho = k_\ell \cos\theta$ is the wavenumber in the horizontal and vertical direction respectively. The total field u after the scattering consists of the incident wave u^i and the diffracted wave u^s. For each sample $\zeta \in \Omega$, the total field u satisfies

$$\Delta u(\zeta;x) + k_0^2 \varepsilon_{r,j} u(\zeta;x) = 0 \qquad \text{for } x \in D_j(\zeta), j = 1,2,\cdots,\ell. \tag{2.3}$$

Along the interfaces $\Gamma_j(\zeta)=\{(x_1,x_2)\,|\,0<x_1<\Lambda_1, x_2=f_j(\zeta;x_1)\}$ for $j=2,\cdots,\ell$, there hold

$$u_+(\zeta;x_1,f_j(\zeta,x_1)) = u_-(\zeta;x_1,f_j(\zeta,x_1)), \tag{2.4}$$

$$\partial_\nu u_+(\zeta;x_1,f_j(\zeta,x_1)) = \partial_\nu u_-(\zeta;x_1,f_j(\zeta,x_1)), \tag{2.5}$$

which follow from the continuity of the electric field and magnetic field. In the above, ν denotes the unit normal vector along Γ_j pointing toward D_j, $u_\pm$ and $\partial_\nu u_\pm$ denote the limits of u and $\partial_\nu u$ from above and below the surface, respectively. In addition, due to periodicity of the medium along the x_1 direction, we impose the quasi-boundary condition on the boundary walls of the periodic cell (cf. [2]):

$$u(\zeta;\Lambda,x_2)=e^{i\tau\Lambda}u(\zeta;0,x_2) \quad \text{for } x_2>f_1(\zeta;0), \tag{2.6}$$

in which τ is the horizontal wavenumber defined above. For a perfectly conducting contact layer D_1 such as aluminum depicted in Figure 1), there holds

$$u(\zeta;x_1,f_1(\zeta;x_1))=0, \quad 0<x_1<\Lambda, \tag{2.7}$$

along the boundary Γ_1. This implies that the optical light is totally reflected to the cell and no light is transmitted through Γ_1.

By virtue of the quasi-periodicity boundary condition, the solution to (2.3) - (2.7) can be expressed as a sum of a Fourier series. In particular, in the domain D_ℓ, the diffracted field u^s attains the so-called Rayleigh expansion (cf. [2,8]):

$$u^s(\zeta;x_1,x_2)=\sum_{n=-\infty}^{\infty}\hat{u}_n^s(\zeta;b)\,e^{i\kappa_n x_1+i\eta_n(x_2-b)} \quad \text{for } x_2\geq b, \tag{2.8}$$

where $b>\max\limits_{-\infty<x_1<\infty} f_\ell(x_1)$ is a constant, $\kappa_n:=\tau+\dfrac{2\pi n}{\Lambda}$ for $n\in\mathbb{Z}$, and

$$\eta_n=\begin{cases}\sqrt{k_\ell^2-\kappa_n^2}, & k_\ell>\kappa_n,\\[2ex] i\sqrt{\kappa_n^2-k_\ell^2}, & k_\ell<\kappa_n.\end{cases} \tag{2.9}$$

The Fourier mode $e^{i\kappa_n x_1+i\eta_n(x_2-b)}$ is called the nth diffraction order and the corresponding Fourier coefficient $\hat{u}_n^s(\zeta;b)$ is defined by

$$\hat{u}_n^s(\zeta;b)=\frac{1}{\Lambda}\int_0^\Lambda u^s(\zeta;x_1,b)e^{-i\kappa_n x_1}\,dx_1. \tag{2.10}$$

Here we assume that $\kappa_n\neq k_\ell$ to exclude resonances. Then we can introduce the Dirichlet-to-Neumann map T on the line $x_2=b$ as

$$\frac{\partial u^s}{\partial x_2}(\zeta;x_1,b)=\sum_{n=-\infty}^{\infty} i\eta_n\hat{u}_n^s(\zeta;b)e^{i\kappa_n x_1}=:T[u^s(\zeta;x_1,b)]. \tag{2.11}$$

Since $u=u^i+u^s$, there holds

$$\frac{\partial u}{\partial x_2}(\zeta;x_1,b)=T(u(\zeta;x_1,b))+g, \tag{2.12}$$

where $g=-2i\rho e^{i\tau x_1-i\rho b}$.

Let $\Gamma(\zeta)=\bigcup_{j=2}^{\ell}\Gamma_j(\zeta)$ and

$$D(\zeta):=\{(x_1,x_2):0<x_1<\Lambda_1, f_1(\zeta;x_1)<x_2<b\}.$$

In light of (2.3) - (2.7) and (2.12), for each sample ζ, the total field u satisfies the following boundary value problem in the domain D:

$$\begin{cases} \Delta u(\zeta;\cdot)+k_0^2\varepsilon_r u(\zeta;\cdot)=0 & \text{in } D(\zeta)\setminus\Gamma(\zeta),\\ u(\zeta;\Lambda,x_2)=e^{i\tau\Lambda}u(\zeta;0,x_2), & f_1(\zeta;0)<x_2<b,\\ u(\zeta;x_1,f_1(\zeta;x_1))=0, & 0<x_1<\Lambda,\\ \dfrac{\partial u}{\partial x_2}(\zeta;x_1,b)=T(u(\zeta;x_1,b))+g, & 0<x_1<\Lambda. \end{cases} \tag{2.13}$$

In addition, u satisfies the conditions (2.4) - (2.5) along the interfaces.

2.2 Representation of random surfaces

For each random interface Γ_j, we assume that its profile function $f_j=f_j(\zeta;x_1)$ is a stationary random process for $x_1\in[0,\Lambda]$, with a continuous and bounded covariance function $C_j(x_1,\tilde{x}_1)=c_j(x_1-\tilde{x}_1)$. We consider the Gaussian type covariance function with

$$c_j(x_1-\tilde{x}_1)=\left(\alpha_j^{(1)}\right)^2\exp\left(-|x_1-\tilde{x}_1|^2/\left(\alpha_j^{(2)}\right)^2\right),$$

where $\alpha_j^{(1)}$ is the root mean square and $\alpha_j^{(2)}$ is the correlation length of the surface $\Gamma_j(\zeta)$ satisfying $0<\alpha_j^{(2)}\ll\Lambda$. Such a covariance function is usually used for the modeling of rough surfaces [17].

By the Karhunen–Loève expansion (cf. [14]), the random process $f_j(\zeta;x_1)$ can be represented as

$$f_j(\zeta;x_1)=f_j^a+\sum_{p=1}^{\infty}\sqrt{\lambda_{jp}}\,\xi_{jp}\varphi_{jp}(x_1),$$

where f_j^a is the average height of f_j, ξ_{jp} are mutually uncorrelated random variables with zero mean and unit covariance, λ_{jp} and φ_{jp} $(p=1,2,\cdots,)$ are the eigenvalues and eigenfunctions of covariance operator

$$[K\varphi](x_1):=\int_0^{\Lambda}c_j(x_1-\tilde{x}_1)\,\varphi(\tilde{x}_1)d\tilde{x}_1.$$

Since the covariance function $c_j(x_1)$ is even, we expand it as

$$c_j(x_1) = \left(\alpha_j^{(1)}\right)^2 \left[\frac{\widehat{c}_{j0}}{2} + \sum_{p=1}^{\infty} \widehat{c}_{jp} \cos\left(\frac{2p\pi x_1}{\Lambda}\right)\right] \quad \text{for } x_1 \in [0,\Lambda],$$

where $\widehat{c}_{j0}, \widehat{c}_{j1}, \widehat{c}_{j2}, \cdots$, are the Fourier cosine expansion coefficients of the function $\exp\left(-x_1^2/\left(\alpha_j^{(2)}\right)^2\right)$. It can be shown that the covariance operator attains the eigenvalues

$$\lambda_{jp} = \frac{\left(\alpha_j^{(1)}\right)^2 \Lambda \hat{c}_{jp}}{2}, \quad p = 0,1,2,\cdots.$$

The corresponding eigenfunctions are

$$\varphi_{jp}(x_1) = \begin{cases} \sqrt{\dfrac{1}{\Lambda}}, & p = 0, \\ \sqrt{\dfrac{2}{\Lambda}} \cos\left(\dfrac{2p\pi x_1}{\Lambda}\right), & p > 1 \text{ and even}, \\ \sqrt{\dfrac{2}{\Lambda}} \sin\left(\dfrac{2p\pi x_1}{\Lambda}\right), & p > 1 \text{ and odd}, \end{cases}$$

for all j. Hence the Karhunen–Loève representation of the random process $f_j(\zeta; x_1)$ is given by

$$\begin{aligned} f_j(\zeta; \alpha_j; x_1) = f_j^a &+ \sqrt{\lambda_{j0}}\, \xi_0(\zeta) \sqrt{\frac{1}{\Lambda}} \\ &+ \sum_{p=1}^{\infty} \sqrt{\lambda_{jp}} \left[\xi_p^s(\zeta) \sqrt{\frac{2}{\Lambda}} \sin\left(\frac{2p\pi x_1}{\Lambda}\right) + \xi_p^c(\zeta) \sqrt{\frac{2}{\Lambda}} \cos\left(\frac{2p\pi x_1}{\Lambda}\right)\right], \end{aligned} \tag{2.14}$$

where ξ_0, ξ_p^s and ξ_p^c are mutually uncorrelated random variables with zero mean and unit covariance. $\alpha_j = (\alpha_j^{(1)}, \alpha_j^{(2)})$ represents the statistical parameters of the interface. We express the explicit dependence of f_j on α_j here and afterwards when necessary. In particular, when $f_j = f_j(\zeta; x_1)$ is a stationary Gaussian process, ξ_0, ξ_p^s and ξ_p^c are independent and identically distributed Gaussian random variables with zero mean and unit covariance.

A finite-term Karhunen-Loève expansion is used in the computation so that the remaining terms are sufficiently small. Since the eigenvalues $\{\lambda_{jp}\}_{j=0}^{\infty}$ converge to 0 fast for the given smooth kernel $c(x_1 - \tilde{x}_1)$, such an approximation yields high-order accuracy with a small number of terms in the expansion. Therefore, here and henceforth, for simplicity we use a finite-term approximation of (2.14) with $p \le P_0$. By letting $\lambda_{jp} = \left(\alpha_j^{(1)}\right)^2 \overline{\lambda}_{jp}$

with $\overline{\lambda}_{jp} = \dfrac{\Lambda \hat{c}_{jp}}{2}$, we express the profile of the random surface by

$$f_j(\zeta;\alpha_j;x_1) = f_j^a + \alpha_j^{(1)} \cdot \bar{f}_j(\zeta;\alpha_j^{(2)};x_1), \tag{2.15}$$

where

$$\begin{aligned} \bar{f}_j(\zeta;\alpha_j^{(2)};x_1) &= \sqrt{\overline{\lambda}_{j0}}\xi_0(\zeta)\sqrt{\frac{1}{\Lambda}} + \sum_{p=1}^{P_0}\sqrt{\overline{\lambda}_{jp}}\left[\xi_p^s(\zeta)\sqrt{\frac{2}{\Lambda}}\sin\left(\frac{2p\pi x_1}{\Lambda}\right)\right. \\ &\quad \left. + \xi_p^c(\zeta)\sqrt{\frac{2}{\Lambda}}\cos\left(\frac{2p\pi x_1}{\Lambda}\right)\right], \end{aligned} \tag{2.16}$$

and it is independent of the root mean square $\alpha_j^{(1)}$. For each random sample, $f_j(\zeta;\alpha_j,\cdot)$ is a smooth function and depends continuously on the statistical parameters α_j.

2.3 Optimal design problems

For each sample $\zeta \in \Omega$, in light of the Rayleigh expansion (2.8), the diffracted field can be rewritten as

$$u^s(\zeta;\cdot) = \sum_{n=-\infty}^{\infty} r_n(\zeta)\, e^{i\kappa_n x_1 + i\eta_n x_2},$$

where the reflection coefficient $r_n(\zeta) = \hat{u}_n^s(\zeta;b)e^{-i\eta_n b}$, and $\hat{u}_n^s$ are the Fourier coefficients of the diffracted field u^s as defined in (2.10). Since $u = u^i + u^s$, $r_n(\zeta)$ can also be written as

$$r_n(\zeta) = \begin{cases} \hat{u}_n(\zeta;b)e^{-i\eta_n b}, & n \neq 0 \\ \hat{u}_n(\zeta;b)e^{-i\rho b} - e^{-2ik_\ell b}, & n = 0, \end{cases} \tag{2.17}$$

where $\hat{u}_n(\zeta;b)$ are the Fourier coefficients of the total field $u(\zeta;\cdot)$ on $x_2 = b$.

Let $\mathcal{N} := \{n \in \mathbb{Z} \,|\, k_\ell^2 - \kappa_n^2 > 0\}$ be the set of indices for all propagating modes in the Rayleigh expansion. The goal of optimal design is to trap the energy in the layers $D_1, \cdots, D_{\ell-1}$ as much as possible. In other words, we aim to minimize the energy that is being reflected to D_ℓ. Let $\boldsymbol{\alpha} = (\alpha_1, \cdots, \alpha_\ell)^\top$ be the design variables, where $\alpha_j = (\alpha_j^{(1)}, \alpha_j^{(2)})$ are the statistical parameters of the interface Γ_j for $j = 1, \cdots, \ell$. Using the reflection coefficients above, the reflectivity associated with the optical structure for each sample ζ is defined by

$$R(\zeta;\boldsymbol{\alpha}) = \sum_{n \in \mathcal{N}} \frac{\eta_n}{\eta_0} |r_n(\zeta)|^2,$$

where η_n is defined in (2.9). The mean reflectivity is

$$E[R(\zeta;\boldsymbol{\alpha})] := \int_\Omega \sum_{n \in \mathcal{N}} \frac{\eta_n}{\eta_0} |r_n(\zeta)|^2 \, dP(\zeta), \tag{2.18}$$

in which Ω and P denotes the random sample space and the probability measure, respectively.

Let $Q(\boldsymbol{\alpha}) := E[R(\zeta;\boldsymbol{\alpha})]$, the optimal design problem for the fixed wavenumber k_0 is to minimize the mean reflectivity $Q(\boldsymbol{\alpha})$ by solving the following stochastic optimization problem over an admissible set $U_{\boldsymbol{\alpha}} := \Big((0,\alpha_1^{\max}) \times (0,\alpha_2^{\max})\Big)^{\ell}$:

$$\text{Problem (I)} \qquad \min_{\boldsymbol{\alpha}\in U_{\boldsymbol{\alpha}}} Q(\boldsymbol{\alpha}). \tag{2.19}$$

Since the solar frequency spectrum ranges from 300nm to about 3000nm, and the angle of the incidence for the incoming light changes during the daytime, it is also important to investigate the corresponding optimization problems in these realistic scenarios. In the case of optimal design over a frequency band, assuming that the wavelength λ for the incident wave is within the range $[\lambda_{min},\lambda_{max}]$, the corresponding stochastic optimization problem is cast as

$$\text{Problem (II)} \qquad \min_{\boldsymbol{\alpha}\in U_{\boldsymbol{\alpha}}} Q(\boldsymbol{\alpha}), \text{ where } Q(\boldsymbol{\alpha}) := E\left[\int_{\lambda_{min}}^{\lambda_{max}} R(\zeta;\boldsymbol{\alpha},\lambda)\, d\lambda\right]. \tag{2.20}$$

Note that in this configuration, the refractive index $\varepsilon_r(\lambda;x)$ is a function of the wavelength λ. Finally, the optimal design problem with multiple incident angles with $\theta \in [\theta_{min},\theta_{max}]$ is formulated as follows:

$$\text{Problem (III)} \qquad \min_{\boldsymbol{\alpha}\in U_{\boldsymbol{\alpha}}} Q(\boldsymbol{\alpha}), \text{ where } Q(\boldsymbol{\alpha}) := E\left[\int_{\theta_{min}}^{\theta_{max}} R(\zeta;\boldsymbol{\alpha},\theta)\, d\theta\right]. \tag{2.21}$$

Both Problem (II) and (III) are computationally more expensive than Problem (I) due to the necessity to sample over the frequency band or at different incident angles. It is computationally formidable by using the gradient descent algorithm in [4] directly.

3 The computation of the gradient $D_{\boldsymbol{\alpha}} R(\zeta;\boldsymbol{\alpha})$

To perform the optimization, one needs to compute the gradient of the objective function. In this section, we derive the gradient $D_{\boldsymbol{\alpha}} R(\zeta;\boldsymbol{\alpha})$ of the reflectivity $R(\zeta;\boldsymbol{\alpha})$ at each sample. The shape derivatives are obtained by analyzing the sensitivity of the reflectivity R upon the perturbation of the interface/surface. Note that Γ_1 at the bottom is the boundary of the structure, while $\Gamma_2,\cdots,\Gamma_\ell$ are interfaces between two layers. Thus the derivations of the shape derivatives are different for the boundary Γ_1 and the rest of interfaces. We present the shape derivative formulas for Γ_1 and Γ_j $(j \geq 2)$ respectively in the following theorem and give the detailed proof in Section 3.2.1 and 3.2.2. The readers are referred to [21] for analysis of derivatives in various shape optimizations.

Theorem 3.1. Denote $D_{\alpha_j} := \left(\frac{\partial}{\partial \alpha_j^{(1)}}, \frac{\partial}{\partial \alpha_j^{(2)}} \right)$ for $j = 1,2,\cdots,\ell$. For each sample ζ,

$$D_{\alpha_1} R(\zeta;\boldsymbol{\alpha}) = \frac{2}{\Lambda} \sum_{n\in\mathcal{N}} \frac{\eta_n}{\eta_0} Re\Big[(\hat{u}_n(\zeta;b) - a_n e^{-2ik_\ell b + i\rho b}) \cdot \int_0^\Lambda \left(\frac{\partial \bar{u}}{\partial \nu} \cdot \frac{\partial u_n^*}{\partial \nu} \nu_2 \right) \cdot D_{\alpha_1} f_1 \, dx_1 \Big], \quad (3.1a)$$

and

$$D_{\alpha_j} R(\zeta;\boldsymbol{\alpha}) = \frac{2k_0^2}{\Lambda} \sum_{n\in\mathcal{N}} \frac{\eta_n}{\eta_0} Re\Big[(\hat{u}_n(\zeta;b) - a_n e^{-2ik_\ell b + i\rho b}) \cdot \overline{(\varepsilon_{r,j} - \varepsilon_{r,j-1})} \cdot \int_0^\Lambda [\bar{u} u_n^*]|_{(x_1,f_j)} \cdot D_{\alpha_j} f_j \, dx_1 \Big], \quad j = 2,\cdots,\ell. \quad (3.1b)$$

Here $a_0 = 1$ and $a_n = 0$ if $n \neq 0$, and $\nu = (\nu_1,\nu_2)^\top$ is the unit normal vector pointing to the interior of D along Γ_1. u is the solution to the forward problem (2.13) and u_n^* solves the following adjoint problem

$$\begin{cases} \Delta u_n^*(\zeta;\cdot) + k_0^2 \overline{\varepsilon_r} u_n^*(\zeta;\cdot) = 0 \ in \ D(\zeta) \setminus \Gamma(\zeta), \\ u_n^*(\zeta;\Lambda,x_2) = e^{i\tau\Lambda} u_n^*(\zeta;0,x_2), \quad f_1(\zeta;0) < x_2 < b, \\ u_n^*(\zeta;x_1,f_1(\zeta;x_1)) = 0, \quad 0 < x_1 < \Lambda, \\ \partial_{x_2} u_n^*(\zeta;x_1,b) = T^*(u(\zeta;x_1,b)) + e^{i\kappa_n x_1}. \end{cases} \quad (3.2)$$

In the above theorem, $[u_n^* \bar{u}]|_{(x_1,f_j)}$ denotes the restriction of $u_n^* \bar{u}$ to the surface $\Gamma_j(\zeta)$. T^* is the adjoint operator of T such that

$$\langle Tu, v \rangle = \langle u, T^* v \rangle,$$

where $\langle \cdot,\cdot \rangle$ stands for the inner product over the function space $L^2(0,\Lambda)$.

3.1 Proof of formula (3.1a)

Let $H_\tau^1(D) := \{u \in H^1(D) : u = 0 \text{ on } \Gamma_1, u(\Lambda,x_2) = e^{i\tau\Lambda} u(0,x_2)\}$, where the function space

$$H^1(D) = \{u(x) : \left(\int_D |u(x)|^2 dx \right)^{\frac{1}{2}} < \infty, \ \left(\int_D |\nabla u(x)|^2 dx \right)^{\frac{1}{2}} < \infty \}.$$

We introduce the bilinear form

$$a(u,w) := \int_D \nabla u \cdot \nabla \bar{w} - k_0^2 \varepsilon_r u \bar{w} \, dx - \langle Tu, w \rangle \quad \text{for } u,w \in H_\tau^1(D).$$

Here $\langle \cdot,\cdot \rangle$ stands for the inner product over the function space $L^2(0,\Lambda)$. Then each random sample ζ, the weak solution $u(\zeta;\cdot) \in H_\tau^1(D)$ for the boundary value problem (2.13) satisfies

$$a(u(\zeta;\cdot),w) = \langle g, w \rangle \quad \text{for all } w \in H_\tau^1(D). \quad (3.3)$$

For each random sample, define the mapping $S:\alpha_1=\left(\alpha_1^{(1)},\alpha_1^{(2)}\right)\to u(\zeta;x_1,b)$, where u is the solution to boundary value problem (2.13). We let $D_{\alpha_1}S:=\left(\frac{\partial S}{\partial\alpha_1^{(1)}},\frac{\partial S}{\partial\alpha_1^{(2)}}\right)$, in which

$$\frac{\partial S}{\partial\alpha_1^{(j)}}=\lim_{\delta\to 0}\frac{S(\alpha^{(1)}+\delta e_j)-S(\alpha^{(1)})}{\delta}\quad \text{for } j=1,2,$$

and e_j is the unit vector.

Lemma 3.2. The derivative $D_{\alpha_1}S$ exits and $\frac{\partial S}{\partial\alpha_1^{(j)}}=u_{j0}(\zeta;x_1,b)$ for $j=1,2$, where u_{j0} solves

$$\begin{cases}\Delta u_{j0}(\zeta;\cdot)+k_0^2\varepsilon_r u_{j0}(\zeta;\cdot)=0 \text{ in } D(\zeta)\setminus\Gamma(\zeta),\\ u_{j0}(\zeta;0,x_2)=e^{i\tau\Lambda}u_{j0}(\zeta;\Lambda,x_2),\\ u_{j0}(\zeta;x_1,f_1(x_1))=-\frac{\partial f_1}{\partial\alpha_1^{(j)}}\frac{\partial u}{\partial\nu}\nu_2;\ 0<x_1<\Lambda,\\ \partial_{x_2}u_{j0}(\zeta;x_1,b)=T(u_{j0}(\zeta;x_1,b)),\end{cases}\tag{3.4}$$

$\nu=(\nu_1,\nu_2)^\top$ is the unit normal vector pointing to D along Γ_1, and u is the solution to boundary value problem (2.13).

Proof. We only provide the proof for $\frac{\partial S}{\partial\alpha_1^{(1)}}$, and the proof for $\frac{\partial S}{\partial\alpha_1^{(2)}}$ is similar. Let $\alpha_1^{(1)}$ be perturbed by a small number δ, then the new root mean square is $\left(\alpha_1^{(1)}\right)^\delta:=\alpha_1^{(1)}+\delta$ and the new boundary becomes $\Gamma_1^\delta:=\{(x_1,x_2):x_2=f_1^\delta(\zeta;x_1)\}$, where $f_1^\delta=f_1+\delta\cdot\frac{\partial f_1}{\partial\alpha_1^{(1)}}+O(\delta^2)$. For simplicity of the notation, we introduce the vector function $W(x)\in C_0^2(\Gamma_1;\mathbb{R}^2)$ such that $\delta\cdot W(x):=[0,f_1^\delta(x_1)-f_1(x_1)]^\top$ for $x\in\Gamma_1$, then the perturbed boundary can be expressed as $\Gamma_1^\delta=\{x+\delta\cdot W(x):x\in\Gamma_1\}$.

We denote the domain after the perturbation by D^δ. The perturbed total field u^δ satisfies

$$\begin{cases}\Delta u^\delta(\zeta;\cdot)+k_0^2\varepsilon_r u^\delta(\zeta;\cdot)=0 \text{ in } D^\delta(\zeta)\setminus\Gamma(\zeta),\\ u^\delta(\zeta;\Lambda,x_2)=e^{i\tau\Lambda}u^\delta(\zeta;0,x_2),\\ u^\delta(\zeta;x_1,f_1(\zeta;x_1))=0;\ 0<x_1<\Lambda,\\ \partial_{x_2}u^\delta(\zeta;x_1,b)=T(u^\delta(\zeta;x_1,b))+g.\end{cases}\tag{3.5}$$

The weak solution u^δ for the above boundary value problem satisfies

$$a^\delta(u^\delta(\zeta;\cdot),w^\delta)=\langle g,w^\delta\rangle\tag{3.6}$$

for all $w^\delta \in H_0^1(D^\delta)$, where

$$a^\delta(u^\delta(\zeta;\cdot),w^\delta) = \int_{D^\delta} \nabla u^\delta(\zeta;\cdot)\cdot\nabla\overline{w^\delta} - k_0^2\varepsilon_r u^\delta(\zeta;\cdot)\overline{w^\delta}\,dx - \langle Tu^\delta(\zeta;\cdot),w^\delta\rangle.$$

Let us extend the definition of $W(x)$ to the closure of the whole domain D such that $W \in C^2(\bar{D};\mathbb{R}^2)$ and $W(x)=0$ on the boundary $x_2 = b$. Correspondingly, we introduce a map ψ from D to D^δ by letting $x = \psi(y) = y + W(y)$ for $y \in D$. The inverse map of ψ is denoted as $\phi(x)$, which maps D^δ to D. Let $\tilde{u}^\delta(y) = u^\delta(\psi(y))$, $\tilde{w}^\delta = w^\delta(\psi(y))$, then $\tilde{u}^\delta$ and $\tilde{w}$ are defined on D. It is straightforward to show that $\dfrac{\partial u^\delta}{\partial x_1} = \sum\limits_{m=1}^{2} \dfrac{\partial \tilde{u}^\delta}{\partial y_m}\dfrac{\partial \phi_m}{\partial x_1}$, where ϕ_1,ϕ_2 are the two components of the mapping ϕ. By change of variables, we obtain

$$a^\delta(u^\delta(\zeta;\cdot),w^\delta) = \int_D \Big[\sum_{m,n=1}^{2} b_{mn}\frac{\partial \tilde{u}^\delta(\zeta;\cdot)}{\partial y_m}\frac{\partial\overline{\tilde{w}^\delta}}{\partial y_n} - k_0^2\varepsilon_r\tilde{u}^\delta(\zeta;\cdot)\overline{\tilde{w}^\delta}\Big]J\,dy - \langle T\tilde{u}^\delta(\zeta;\cdot),\tilde{w}^\delta\rangle$$

where $J = det\nabla\psi$, $b_{mn} = \sum\limits_{i=1}^{2}\dfrac{\partial\phi_m}{\partial x_i}\dfrac{\partial\phi_n}{\partial x_i}$. Define a new bilinear form

$$\tilde{a}^\delta(\tilde{u}^\delta,w) = \int_D \Big[\sum_{m,n=1}^{2} b_{mn}\frac{\partial \tilde{u}^\delta}{\partial y_m}\frac{\partial\overline{w}}{\partial y_n} - k_0^2\varepsilon_r\tilde{u}^\delta\overline{w}\Big]J\,dy - \langle T\tilde{u}^\delta,w\rangle$$

for $\tilde{u}^\delta, w \in H_\tau^1(D)$. Then (3.6) is equivalent to finding $\tilde{u}^\delta \in H_\tau^1(D)$ such that

$$\tilde{a}(\tilde{u}^\delta(\zeta;\cdot),w) = \langle g,w\rangle \tag{3.7}$$

for all $w \in H_\tau^1(D)$.

From (3.3) and (3.7), it is seen that $\tilde{u}^\delta(\zeta;\cdot) - u(\zeta;\cdot)$ satisfies

$$a(\tilde{u}^\delta(\zeta;\cdot)-u(\zeta;\cdot),w) = -\big(\tilde{a}^\delta(\tilde{u}^\delta(\zeta;\cdot),w) - a(\tilde{u}^\delta(\zeta;\cdot),w)\big). \tag{3.8}$$

For the right-hand side,

$$\begin{aligned}\tilde{a}^\delta(\tilde{u}^\delta(\zeta;\cdot),w) - a(\tilde{u}^\delta(\zeta;\cdot),w) = &\int_D \Big[\sum_{m,n=1}^{2} b_{mn}\frac{\partial \tilde{u}^\delta(\zeta;\cdot)}{\partial y_m}\frac{\partial\overline{w}}{\partial y_n} - k_0^2\varepsilon_r\tilde{u}^\delta(\zeta;\cdot)\overline{w}\Big]J\,dy \\ &- \int_D \nabla\tilde{u}^\delta(\zeta;\cdot)\cdot\nabla\bar{w} - k_0^2\varepsilon_r\tilde{u}^\delta(\zeta;\cdot)\bar{w}\,dy.\end{aligned} \tag{3.9}$$

Let $V(x)$ be the leading-order of the vector function $W(x)$ and it is independent of δ. Then it can be calculated that the Jacobian $J = 1+\delta\nabla\cdot V + O(\delta^2)$, and $(b_{mn})J = I - \delta(\tilde{b}_{mn}) + O(\delta^2)$, where I is the 2×2 identity matrix and

$$\tilde{b}_{mn} = \nabla V + (\nabla V)^T - (\nabla\cdot V)I. \tag{3.10}$$

Therefore,

$$a(\tilde{u}^\delta(\zeta;\cdot)-u(\zeta;\cdot),w)=\delta\int_D\sum_{m,n=1}^{2}\tilde{b}_{mn}\frac{\partial\tilde{u}^\delta(\zeta;\cdot)}{\partial y_m}\frac{\partial\overline{w}}{\partial y_n}+k_0^2\varepsilon_r(\nabla\cdot V)u(\zeta;\cdot)\overline{w}dy+O(\delta^2). \quad (3.11)$$

Denote $u'(\zeta;\cdot)=\lim_{\delta\to0}\frac{\tilde{u}^\delta(\zeta;\cdot)-u(\zeta;\cdot)}{\delta}$. Then $u'(\zeta;\cdot)$ satisfies the following variational formulation:

$$a(u'(\zeta;\cdot),w)=\int_D\sum_{m,n=1}^{2}\tilde{b}_{mn}\frac{\partial\tilde{u}^\delta(\zeta;\cdot)}{\partial y_m}\frac{\partial\overline{w}}{\partial y_n}+k_0^2\varepsilon_r(\nabla\cdot V)u(\zeta;\cdot)\overline{w}dy. \quad (3.12)$$

By the formula (3.10), we have

$$\begin{aligned}\sum_{m,n=1}^{2}\tilde{b}_{mn}\frac{\partial u(\zeta;\cdot)}{\partial y_m}\frac{\partial\overline{w}}{\partial y_n}=&\nabla(V\cdot\nabla\bar{w})\cdot\nabla u(\zeta;\cdot)+\nabla(V\cdot\nabla u(\zeta;\cdot))\cdot\nabla\bar{w}\\&-\nabla\cdot[(\nabla u(\zeta;\cdot)\cdot\nabla\bar{w})V].\end{aligned}$$

By the Green's formula and the boundary condition $u(\zeta;\cdot)=w=0$ on Γ_1, there holds

$$\int_{\Gamma_1}(V\cdot\nabla\bar{w})\frac{\partial u(\zeta;\cdot)}{\partial\nu}-(\nabla u(\zeta;\cdot)\cdot\nabla\bar{w})(V\cdot\nu)ds=0.$$

Therefore, (3.12) can be reduced to

$$\begin{aligned}a(u'(\zeta;\cdot),w)=&\int_D-\nabla(V\cdot\nabla\bar{w})\cdot\nabla u(\zeta;\cdot)+\nabla(V\cdot\nabla u(\zeta;\cdot))\cdot\nabla\bar{w}+k_0^2\varepsilon_r(\nabla\cdot V)u(\zeta;\cdot)\overline{w}dy\\&+\int_{\Gamma_1}(V\cdot\nabla\bar{w})\frac{\partial u(\zeta;\cdot)}{\partial\nu}-(\nabla u(\zeta;\cdot)\cdot\nabla\bar{w})(V\cdot\nu)ds\\=&\int_D k_0^2\varepsilon_r u(\zeta;\cdot)(V\cdot\nabla\bar{w})+\nabla(V\cdot\nabla u(\zeta;\cdot))\cdot\nabla\bar{w}+k_0^2\varepsilon_r(\nabla\cdot V)u(\zeta;\cdot)\overline{w}dy\\=&\int_D\nabla(V\cdot\nabla u(\zeta;\cdot))\cdot\bar{w}-k_0^2\varepsilon_r(V\cdot\nabla u(\zeta;\cdot))\bar{w}dy+\int_D k_0^2\varepsilon_r\nabla\cdot(u(\zeta;\cdot)\bar{w}V)dy.\end{aligned} \quad (3.13)$$

Since $\int_D k_0^2\varepsilon_r\nabla\cdot(u(\zeta;\cdot)\bar{w}V)dy=0$ by the divergence theorem, we obtain

$$a(u'(\zeta;\cdot),w)=\int_D\nabla(V\cdot\nabla u(\zeta;\cdot))\cdot\nabla\bar{w}-k_0^2\varepsilon_r(V\cdot\nabla\bar{u}(\zeta;\cdot))\bar{w}dy \text{ for any } w\in H^1_\tau(D)\cap H^2(D).$$

This implies that u' is a weak solution of the following boundary value problem:

$$\begin{cases}\Delta u'(\zeta;\cdot)+k_0^2\varepsilon_r u'(\zeta;\cdot)=(\Delta+k_0^2\varepsilon_r)(V-\nabla u) \text{ in } D(\zeta)\setminus\Gamma(\zeta),\\ u'(\zeta;\Lambda,x_2)=e^{i\tau\Lambda}u'(\zeta;0,x_2),\\ u'(\zeta;x_1,f_1(x_1))=0;\ 0<x_1<\Lambda,\\ \partial_{x_2}u'(\zeta;x_1,b)=T(u'(\zeta;x_1,b)).\end{cases}$$

Let $u_{10}=u'-V\cdot\nabla u$, then $u_{10}=u'$ on $x_2=b$, and u_{10} satisfies

$$\begin{cases} \Delta u_{10}(\zeta;\cdot)+k_0^2\varepsilon_r u_{10}(\zeta;\cdot)=0 \text{ in } D(\zeta)\setminus\Gamma(\zeta), \\ u_{10}(\zeta;\Lambda,x_2)=e^{i\tau\Lambda}u_{10}(\zeta;0,x_2), \\ u_{10}(\zeta;x_1,f_1(x_1))=\dfrac{\partial f_1}{\partial\alpha_1^{(1)}}\dfrac{\partial u}{\partial\nu}\nu_2;\ 0<x_1<\Lambda, \\ \partial_{x_2}u_{10}(\zeta;x_1,b)=T(u_{10}(\zeta;x_1,b)). \end{cases}$$

This completes the proof of Lemma 3.2.

Next, let us prove formula (3.1a). From the definition of the reflectivity $R(\zeta;\boldsymbol{\alpha})=\sum_{n\in\mathcal{N}}\dfrac{\eta_n}{\eta_0}|r_n(\zeta)|^2$, we have

$$\frac{\partial R(\zeta;\boldsymbol{\alpha})}{\partial\alpha_1^{(1)}}=2\sum_{n\in\mathcal{N}}\frac{\eta_n}{\eta_0}\mathrm{Re}\Big[r_n\frac{\partial\bar{r}_n}{\partial\alpha_1^{(1)}}\Big],$$

where

$$r_n(\zeta)=\begin{cases} \hat{u}_n(\zeta;b)e^{-i\eta_n b}, & n\neq 0 \\ \hat{u}_n(\zeta;b)e^{-i\rho b}-e^{-2ik_0q_\ell b}, & n=0. \end{cases}$$

From a direct calculation, it follows that

$$\frac{\partial r_n(\zeta)}{\partial\alpha_1^{(1)}}=\frac{\partial\hat{u}_n(\zeta;b)}{\partial\alpha_1^{(1)}}e^{-i\eta_n b}.$$

Applying Lemma 3.2, we obtain $\dfrac{\partial u(\zeta;b)}{\partial\alpha_1^{(1)}}=\lim\limits_{\delta\to 0}\dfrac{u^\delta(\zeta;b)-u(\zeta;b)}{\delta}=u_{01}(\zeta;b)$. Thus

$$r_n\frac{\partial\bar{r}_n}{\partial\alpha_1^{(1)}}=\begin{cases} \hat{u}_n(\zeta;b)\cdot\dfrac{1}{\Lambda}\displaystyle\int_0^\Lambda e^{i\kappa_n x_1}\overline{u_{01}(\zeta;x_1,b)}\,dx_1, & n\neq 0 \\ \big(\hat{u}_n(\zeta;b)-e^{-2ik_0q_\ell b+i\rho b}\big)\cdot\dfrac{1}{\Lambda}\displaystyle\int_0^\Lambda e^{i\kappa_n x_1}\overline{u_{01}(\zeta;x_1,b)}\,dx_1, & n=0. \end{cases} \tag{3.14}$$

Multiplying the differential equation in the adjoint problem (3.2) by $\overline{u_{01}(\zeta;\cdot)}$ and multiplying the complex conjugate of the differential equation in (3.4) by $u_n^*(\zeta;\cdot)$, and integrating over the domain D_j for $j=1,\cdots,\ell$, we have

$$\int_{D_j}(\Delta u_n^*(\zeta;\cdot)+k_0^2\overline{\varepsilon_r}u_n^*(\zeta;\cdot))\overline{u_{01}(\zeta;\cdot)}-u_n^*(\zeta;\cdot)\overline{(\Delta u_{01}(\zeta;\cdot)+k_0^2\varepsilon_r u_{01}(\zeta;\cdot))}\,dx=0;\quad j=1,\cdots,\ell.$$

Applying the Green's formula for the above equations and adding them together, we obtain

$$-\int_0^\Lambda ([0,\frac{\partial f_1}{\partial \alpha_1^{(1)}}]^\top\cdot\nu)\left[\frac{\partial\overline{u(\zeta;\cdot)}}{\partial\nu}\cdot\frac{\partial u_n^*(\zeta;\cdot)}{\partial\nu}\right]dx_1$$
$$+\int_0^\Lambda\overline{u_{01}(\zeta;\cdot)}\left(T^*(u_n^*(\zeta;\cdot)+e^{i\kappa_n x_1})\right)-u_n^*(\zeta;\cdot)T(u_{01}(\zeta;\cdot))dx_1=0,$$

where we have used the boundary conditions in the boundary value problems (3.2) and (3.4).

Since T^* is the adjoint operator of T, there holds

$$\int_0^\Lambda e^{i\kappa_n x_1}\overline{u_{01}(\zeta;x_1,b)}\,dx_1=\int_0^\Lambda\left(\frac{\partial\overline{u(\zeta;\cdot)}}{\partial\nu}\cdot\frac{\partial u_n^*(\zeta;\cdot)}{\partial\nu}\nu_2\right)\frac{\partial f_1}{\partial\alpha_1^{(1)}}dx_1.$$

Substituting into (3.14) leads to

$$\frac{\partial R}{\partial\alpha_1^{(1)}}=\frac{2}{\Lambda}\sum_{n\in\mathcal{N}}\frac{\eta_n}{\eta_0}Re\Big[(\hat{u}_n(\zeta;b)-a_ne^{-2ik_0q_\ell b+i\rho b})\cdot\int_0^\Lambda\left(\frac{\partial\overline{u(\zeta;\cdot)}}{\partial\nu}\cdot\frac{\partial u_n^*(\zeta;\cdot)}{\partial\nu}\nu_2\right)\frac{\partial f_1}{\partial\alpha_1^{(1)}}dx_1\Big].$$

Therefore,

$$D_{\alpha_1}R=\frac{2}{\Lambda}\sum_{n\in\mathcal{N}}\frac{\eta_n}{\eta_0}Re\Big[(\hat{u}_n(\zeta;b)-a_ne^{-2ik_0q_\ell b+i\rho b})\cdot\int_0^\Lambda\left(\frac{\partial\overline{u(\zeta;\cdot)}}{\partial\nu}\cdot\frac{\partial u_n^*(\zeta;\cdot)}{\partial\nu}\nu_2\right)\cdot D_{\alpha_1}f_1\,dx_1\Big].$$

3.2 Proof of formula (3.1b)

To prove (3.1b), we need to derive the perturbation of the reflectivity δR due to the perturbation of the interface by δf_j induced by a small perturbation of $\alpha_j^{(1)}$ or $\alpha_j^{(2)}$ for $j=2,\cdots,\ell$. When the interface Γ_j is perturbed as $f_j^\delta:=f_j+\delta f_j$, the permittivity ε in D_j becomes $\varepsilon_r^\delta:=\varepsilon_r+\delta\varepsilon_r$. It is observed that for any test function $v\in L^2(D)$, the inner product

$$(v,\delta\varepsilon_r):=\int_D v(x)\,\overline{\delta\varepsilon_r}(x)\,dx=\int_{\text{symdiff}(D_j,D_j^\delta)}v(x)\,\overline{\delta\varepsilon_r}(x)\,dx.$$

Here D_j and D_j^δ are the layers with the interfaces f_j and f_j^δ, respectively, and the symmetric difference of the two sets D_j and D_j^δ is given by

$$\text{symdiff}(D_j,D_j^\delta)=(D_j\cup D_j^\delta)\setminus(D_j\cap D_j^\delta).$$

Since the relative permittivity of the domain D_{j-1} and D_j are $\varepsilon_{r,j-1}$ and $\varepsilon_{r,j}$, respectively, the above inner product can be simplified as

$$(v,\delta\varepsilon_r)=\int_0^\Lambda v(x_1,f_j(x_1))\,\overline{(\varepsilon_{r,j-1}-\varepsilon_{r,j})}\cdot\delta f_j\,dx \tag{3.15}$$

for an infinitesimal δf.

Let δu denote the perturbation of the total field. As a result of perturbation analysis, δu satisfies the following equations:

$$\begin{cases} \Delta\delta u(\zeta;\cdot)+k_0^2\varepsilon_r\delta u(\zeta;\cdot)=-k_0^2\delta\varepsilon_r u(\zeta;\cdot) & \text{in } D(\zeta)\setminus\Gamma(\zeta),\\ \delta u(\zeta;\Lambda,x_2)=e^{i\tau\Lambda}\delta u(\zeta;0,x_2), & 0<x_2<b,\\ \delta u(\zeta;x_1,f_1(\zeta;x_1))=0, & 0<x_1<\Lambda,\\ \dfrac{\partial\delta u}{\partial x_2}(\zeta;x_1,b)=T(\delta u(\zeta;x_1,b)) & 0<x_1<\Lambda. \end{cases} \tag{3.16}$$

Multiplying the differential equation in the adjoint problem (3.2) by $\overline{\delta u(\zeta;\cdot)}$ and the differential equation in (3.16) by $\overline{u_n^*(\zeta;\cdot)}$, and integrating over the domain D_j for $j=1,\cdots,\ell$, it follows that

$$\begin{aligned}&\int_{D_j}(\Delta u_n^*(\zeta;\cdot)+k_0^2\overline{\varepsilon_r}u_n^*(\zeta;\cdot))\,\overline{\delta u(\zeta;\cdot)}-u_n^*(\zeta;\cdot)\,\overline{(\Delta\delta u(\zeta;\cdot)+k_0^2\varepsilon_r\delta u(\zeta;\cdot))}\,dx\\ =&\int_{D_j}u_n^*(\zeta;\cdot)k_0^2\overline{\delta\varepsilon_r u(\zeta;\cdot)}\,dx,\quad j=1,\cdots,\ell.\end{aligned}$$

Applying the Green's formula on the left-hand side and adding all the equations together yields

$$\begin{aligned}&\int_{\Gamma_j(\zeta)}(\partial_\nu u_n^*(\zeta;\cdot))_-\overline{(\delta u(\zeta;\cdot))_-}-(u_n^*(\zeta;\cdot))_-\overline{(\partial_\nu\delta u(\zeta;\cdot))_-}\,ds\\ &+\int_{\Gamma_j(\zeta)}(u_n^*(\zeta;\cdot))_+\overline{(\partial_\nu\delta u(\zeta;\cdot))_+}-(\partial_\nu u_n^*(\zeta;\cdot))_+\overline{(\delta u(\zeta;\cdot))_+}\,ds\\ &+\int_0^\Lambda e^{i\kappa_n x}\,\overline{\delta u(\zeta;x_1,b)}\,dx_1=k_0^2\int_D\bar\delta\varepsilon_r u(\bar\zeta;\cdot)u_n^*(\zeta;\cdot)\,dx,\end{aligned}$$

where we have used the boundary conditions in (3.2) and (3.16). By the continuity conditions along the interface $\Gamma_j(\zeta)$, this can be further reduced to the following:

$$\int_0^\Lambda e^{i\kappa_n x}\,\overline{\delta u(\zeta;x_1,b)}\,dx_1=k_0^2\int_D\bar\delta\varepsilon_r u(\bar\zeta;\cdot)u_n^*(\zeta;\cdot)\,dx. \tag{3.17}$$

Now,

$$\begin{aligned} R^{\delta}(\zeta;\boldsymbol{\alpha}) &= \sum_{n\in\mathcal{N}} \frac{\eta_n}{\eta_0} |r_n+\delta r_n|^2 \\ &= \sum_{n\in\mathcal{N}} \frac{\eta_n}{\eta_0} \Big\{ |r_n|^2 + 2\mathrm{Re}[r_n\overline{\delta r_n}] + |\delta r_n|^2 \Big\}. \end{aligned}$$

From the definition of (2.17), it follows that $\delta r_n = O(\delta u)$ where δu is the perturbation of u. Due to the perturbation analysis of the boundary value problem (2.13), we have $\delta u = O(\delta\varepsilon_r)$ and $\delta\varepsilon_r = (\varepsilon_{r,1}-\varepsilon_{r,2})\cdot\delta f_j$. Then it follows $|\delta r_n|^2 = O((\delta f_j)^2)$. We have

$$R^{\delta}(\zeta;\boldsymbol{\alpha}) = R(\zeta;\boldsymbol{\alpha}) + 2\sum_{n\in\mathcal{N}} \frac{\eta_n}{\eta_0} Re[r_n\overline{\delta r_n}] + O((\delta f_j)^2).$$

The perturbation $\delta R := R^{\delta} - R$ is given by

$$\delta R = 2\sum_{n\in\mathcal{N}} \frac{\eta_n}{\eta_0} \mathrm{Re}[r_n\overline{\delta r_n}] + O((\delta f_j)^2). \tag{3.18}$$

For each term $r_n\overline{\delta r_n}$, by virtue of (2.17), it follows that

$$r_n\overline{\delta r_n} = \begin{cases} \hat{u}_n(\zeta;b)\cdot\dfrac{1}{\Lambda}\displaystyle\int_0^{\Lambda} e^{i\kappa_n x_1}\,\overline{\delta u(\zeta;x_1,b)}\,dx_1, & n\neq 0 \\ \big(\hat{u}_n(\zeta;b) - e^{-2ik_\ell b + i\rho b}\big)\cdot\dfrac{1}{\Lambda}\displaystyle\int_0^{\Lambda} e^{i\kappa_n x_1}\,\overline{\delta u(\zeta;x_1,b)}\,dx_1, & n=0. \end{cases} \tag{3.19}$$

Therefore, substituting (3.17) into (3.19) yields

$$r_n\overline{\delta r_n} = \begin{cases} \hat{u}_n(\zeta;b)\cdot\dfrac{k_0^2}{\Lambda}\displaystyle\int_D \bar{\delta\varepsilon}_r\bar{u}u_n^*\,dx, & n\neq 0, \\ \big(\hat{u}_n(\zeta;b) - e^{-2ik_\ell b + i\rho b}\big)\cdot\dfrac{k_0^2}{\Lambda}\displaystyle\int_D \bar{\delta\varepsilon}_r\bar{u}u_n^*\,dx, & n=0. \end{cases} \tag{3.20}$$

As such

$$\delta R = \frac{2k_0^2}{\Lambda}\sum_{n\in\mathcal{N}} \frac{\eta_n}{\eta_0} \mathrm{Re}\Big[(\hat{u}_n(\zeta;b) - \alpha_n e^{-2ik_\ell b + i\rho b})\cdot\int_D \bar{\delta\varepsilon}_r\bar{u}u_n^*\,dx\Big] + O(\delta f_j^2).$$

Using (3.15), we arrive at

$$\delta R = \frac{2k_0^2}{\Lambda}\sum_{n\in\mathcal{N}} \frac{\eta_n}{\eta_0} \mathrm{Re}\Big[(\hat{u}_n(\zeta;b) - \alpha_n e^{-2ik_\ell b + i\rho b})\cdot\overline{(\varepsilon_{r,1}-\varepsilon_{r,2})}\cdot\int_0^{\Lambda} [\bar{u}u_n^*]|_{(x_1,f_j)}\cdot\delta f_j\,dx_1\Big] + O(\delta f^2).$$

The desired formula (3.1b) for $D_{\alpha_j}R$ $(j=2,\cdots,\ell)$ then follows by the chain rule.

4 The stochastic gradient descent method for the optimal design problems

4.1 The computational algorithm

To minimize $Q(\boldsymbol{\alpha}) = E[R(\zeta;\boldsymbol{\alpha})]$, the full gradient descent method applies the iteration

$$\boldsymbol{\alpha}^{(n+1)} = \boldsymbol{\alpha}^{(n)} - h_n \cdot D_{\boldsymbol{\alpha}} Q(\boldsymbol{\alpha}^{(n)}), \tag{4.1}$$

where h_n is the step length and $D_{\boldsymbol{\alpha}} Q(\boldsymbol{\alpha}^{(n)})$ is the gradient of $Q(\boldsymbol{\alpha})$ with respect to $\boldsymbol{\alpha}$. If the Monte Carlo method is used to sample the probability space, then

$$D_{\boldsymbol{\alpha}} Q(\boldsymbol{\alpha}^{(n)}) = E\left[D_{\boldsymbol{\alpha}} R(\zeta;\boldsymbol{\alpha}^{(n)})\right] \approx \frac{1}{M_C} \sum_{m=1}^{M_C} D_{\alpha} R(\zeta_m;\alpha^{(n)}).$$

Usually the sampling size M_C needs to be very large to obtain reasonably accurate approximation, and the computation of each $D_{\alpha} R(\zeta_m;\alpha^{(n)})$ requires solving the boundary value problem (2.13) and the adjoint problems (3.2). Therefore, computing the full gradient $D_{\boldsymbol{\alpha}} Q(\boldsymbol{\alpha}^{(n)})$ is very expensive during the iteration process.

Here we employ the stochastic gradient descent method to solve the optimization problems (I)-(III). The stochastic gradient descent method plays a significant role in solving large-scale modern machine learning problems and it is computationally efficient when the data set is large [7]. Its application for minimizing the objective function $Q(\boldsymbol{\alpha})$ is given by

$$\boldsymbol{\alpha}^{(n+1)} = \boldsymbol{\alpha}^{(n)} - h_n \cdot D_{\boldsymbol{\alpha}} R(\zeta_n;\boldsymbol{\alpha}^{(n)}). \tag{4.2}$$

For each iteration n, the sample ζ_n is randomly chosen. In addition, at each iteration, the numerical method avoids the sampling of the gradient over the probability space and it requires the computation of the gradient $D_{\boldsymbol{\alpha}} R(\zeta_n)$ only for one sample, although the convergence rate is slower than the full gradient algorithm above. The iterative sequence is not determined uniquely by the function $Q(\boldsymbol{\alpha})$, the starting point $\boldsymbol{\alpha}^{(1)}$, and the sequence of step size $\{h_n\}_{n=1}^{\infty}$. Rather, $\{\boldsymbol{\alpha}^{(n)}\}_{n=1}^{\infty}$ is a stochastic process whose behavior is determined by the random sequence $\{\zeta_n\}_{n=1}^{\infty}$.

The stochastic gradient descent method and the full gradient descent method offer different trade-offs in terms of computational cost at each iteration and the convergence rate for the iteration process. The full gradient iteration (4.1) is costly but stable, while the stochastic gradient descent iteration (4.2) is efficient but less stable. The mini-batch stochastic gradient descent method is designed to combine the advantages of both methods by choosing a small random samples of the gradients at each iteration. More precisely, the iteration takes the form

$$\boldsymbol{\alpha}^{(n+1)} = \boldsymbol{\alpha}^{(n)} - h_n \cdot G(\boldsymbol{\alpha}^{(n)}), \tag{4.3}$$

where

$$G(\boldsymbol{\alpha}^{(n)}) = \frac{1}{M_0}\sum_{m=1}^{M_0} D_{\boldsymbol{\alpha}} R(\zeta_m;\boldsymbol{\alpha}^{(n)})$$

is the average of the gradient over a small randomly chosen sample subset $\{\zeta_m\}_{m=1}^{M_0}$. The original stochastic gradient descent iteration (4.2) is a special case when $M_0 = 1$. When $M_0 > 1$, the mini-batch stochastic gradient descent method reduces the variance of the randomly chosen gradient during the iteration process by sampling over a larger set, thus it is more stable than the original algorithm (4.2). Here we apply the iteration formula (4.3) to solve the optimization problems (I)- (III) described as follows.

Algorithm 1 The mini-batch stochastic gradient descent method for Problems (I)- (III)

1: Choose initial guess $\boldsymbol{\alpha}^{(0)}$ and the sample size M_0.
2: **while** The average gradient of the sample set $\|G(\boldsymbol{\alpha}^{(n)})\|_2 >$ tolerance **do**

- Choose a random samples subset $\{\zeta_m\}_{m=1}^{M_0}$.
- For each sample ζ_m, solve the boundary value problem (2.13) and the adjoint problems (3.2) in Section 3.2.
- Compute the gradient $D_{\boldsymbol{\alpha}} R(\zeta_m;\cdot)$ by the formulas (3.1a) and (3.1b) in Section 3.2.
- Set $G(\boldsymbol{\alpha}^{(n)}) = \frac{1}{M_0}\sum_{m=1}^{M_0} D_{\boldsymbol{\alpha}} R(\zeta_m;\boldsymbol{\alpha}^{(n)})$.
- Set $\boldsymbol{\alpha}^{(n+1)} = \boldsymbol{\alpha}^{(n)} - h_n \cdot G(\boldsymbol{\alpha}^{(n)})$, $h_n > 0$.

3: **end while**

4.2 Convergence of the stochastic gradient descent algorithm

In this section, we examine the convergence of the stochastic gradient descent method. Let us focus on the case when the random variables $\{\xi_{j,m}\}_{m=0}^{M}$ in the Karhunen–Loève expansion (2.15) are uniformly distributed over the interval $[-0.5,0.5]$. In what follows, C denotes a generic constant. Its value may vary from step to step but should be clear from the context.

Theorem 4.1. Assume the stochastic gradient descent iterations in **Algorithm 1** satisfies the following conditions:

(1) The step sizes (learning rates) $\{h_n\}_{n=1}^{\infty}$ satisfy $\sum_{n=1}^{\infty} h_n = \infty$ and $\sum_{n=1}^{\infty} h_n^2 < \infty$.

(2) The iteration sequence $\{\boldsymbol{\alpha}^{(n)}\}_{n=1}^{\infty}$ is bounded in the closed region $U_{\boldsymbol{\alpha}} = \Big([0,\beta_1]\times[\beta_2,\Lambda]\Big)^{\ell}$ for certain constants $\beta_1,\beta_2 > 0$.

Then $E\left[\|D_{\boldsymbol{\alpha}}Q(\boldsymbol{\alpha}^{(n)})\|_2^2\right]\to 0$ as $n\to\infty$.

To prove the theorem, we need the following lemma.

Lemma 4.2 ([15], Lemma 1). Let $(a_t)_{t\geq 1}$, $(b_t)_{t\geq 1}$ be two nonnegative real sequences. Assume that $\sum_{t=1}^{\infty} a_t b_t$ converges and $\sum_{t=1}^{\infty} a_t$ diverges, and there exists $K\geq 0$ such that $|b_{t+1}-b_t|\leq Ka_t$. Then b_t converges to 0.

Proof of Theorem 4.1 From the expression (2.15), we have

$$\frac{\partial f_j(\zeta;\alpha_j;\cdot)}{\partial \alpha_j^{(1)}}=\bar{f}_j(\zeta;\alpha_j;\cdot),$$

where $\bar{f}_j$ is given in (2.16). It follows that

$$E\left[\left\|\frac{\partial f_j(\zeta;\alpha_j;x_1)}{\partial \alpha_j^{(1)}}\right\|^2_{L^2([0,\Lambda])}\right]=E\left[\|\bar{f}_j(\zeta;\alpha_j;x_1)\|^2_{L^2([0,\Lambda])}\right]\leq C\sum_{p=0}^{P}|\overline{\lambda}_{jp}|^2.$$

On the other hand, $\dfrac{\partial f_j(\zeta;\alpha_j;x_1)}{\partial \alpha_j^{(1)}}=\alpha_j^{(1)}\cdot\dfrac{\partial \bar{f}_j(\zeta;\alpha_j^{(2)};\cdot)}{\partial \alpha_j^{(2)}}$, and

$$\begin{aligned}\frac{\partial \bar{f}_j(\zeta;\alpha_j^{(2)};x_1)}{\partial \alpha_j^{(2)}} &= \frac{\bar{\lambda}'_{j0}}{2\sqrt{\bar{\lambda}_{j0}}}\xi_0(\zeta)\sqrt{\frac{1}{\Lambda}}+\sum_{p=1}^{P}\frac{\bar{\lambda}'_{jp}}{2\sqrt{\bar{\lambda}_{jp}}}\left[\xi_p^s(\zeta)\sqrt{\frac{2}{\Lambda}}\sin\left(\frac{2p\pi x_1}{\Lambda}\right)\right.\\ &\quad\left.+\xi_p^c(\zeta)\sqrt{\frac{2}{\Lambda}}\cos\left(\frac{2p\pi x_1}{\Lambda}\right)\right],\end{aligned}\tag{4.4}$$

where

$$\bar{\lambda}'_{jp}:=\frac{\partial\bar{\lambda}_{jp}}{\partial\alpha_j^{(2)}}=\frac{\Lambda}{2}\frac{\partial\hat{c}_{jp}}{\partial\alpha_j^{(2)}}\quad\text{for } p=0,1,2,\cdots,P_0.$$

Recall that $\{\hat{c}_{jp}\}_{p=0}^{\infty}$ are the Fourier coefficients of the analytic function $\exp\left(-x_1^2/\left(\alpha_j^{(2)}\right)^2\right)$, thus $\left\{\dfrac{\partial\hat{c}_{jp}}{\partial\alpha_j^{(2)}}\right\}_{p=0}^{\infty}$ are the Fourier coefficients of the function $\dfrac{x_1^2}{(\alpha_j^{(2)})^3}\exp\left(-x_1^2/\left(\alpha_j^{(2)}\right)^2\right)$, which again is analytic for $x_1\in[0,\Lambda]$ and $\alpha_j^{(2)}\in[\beta_2,\Lambda]$. We deduce that

$$E\left[\left\|\frac{\partial f_j(\zeta;x_1)}{\partial \alpha_j^{(2)}}\right\|^2_{L^2([0,\Lambda])}\right]\leq C\left(\alpha_j^{(1)}\right)^2\sum_{p=0}^{P_0}\left|\frac{\lambda'_{jp}}{2\sqrt{\lambda_{jp}}}\right|^2=\frac{\Lambda^2}{8}\left(\alpha_j^{(1)}\right)^2\sum_{p=0}^{P_0}\left|\frac{\hat{c}'_{jp}}{\sqrt{\hat{c}_{jp}}}\right|^2\leq C(P_0),$$

where the constant C depends on P_0. Namely, there holds

$$E\left[\|D_{\alpha_j} f_j(\zeta;x_1)\|_2^2\right] \le C,\ \ j=1,\cdots,\ell. \tag{4.5}$$

Let $p(y_1,\cdots,y_{2P_0+1})$ be the joint probability density function of the multivariate random variable $(\xi_0,\xi_1^s,\cdots,\xi_{P_0}^s,\xi_1^c,\cdots,\xi_{P_0}^c)$. From the continuous dependence of the solution to the boundary value problem (2.13) on the interfaces, u can be viewed as a continuous function of random variables $(\xi_0,\xi_1^s,\cdots,\xi_{P_0}^s,\xi_1^c,\cdots,\xi_{P_0}^c)$. Therefore,

$$\begin{aligned}
&E\left[\|u(\xi_0,\xi_1^s,\cdots,\xi_{P_0}^s,\xi_1^c,\cdots,\xi_{P_0}^c;\cdot)\|_{L^2(D)}^2\right]\\
=&\int_\Omega \|u(\xi_0,\xi_1^s,\cdots,\xi_{P_0}^s,\xi_1^c,\cdots,\xi_{P_0}^c;\cdot)\|_{L^2(D)}^2 dP(\xi_0,\xi_1^s,\cdots,\xi_{P_0}^s,\xi_1^c,\cdots,\xi_{P_0}^c)\\
=&\int_{[-0.5,0.5]^{2P_0+1}} \|u(y_1,\cdots,y_{2P_0+1};\cdot)\|_{L^2(D)}^2 p(y_1,\cdots,y_{2P_0+1})dy_1\cdots dy_{2P_0+1} \le C(P_0).
\end{aligned} \tag{4.6}$$

Similarly, we have

$$E\left[\|u_n^*\|_{L^2(D)}^2\right] \le C,\ E\left[\left\|\frac{\partial u}{\partial \nu}\right\|_{L^2(0,\Lambda)}^2\right] \le C \text{ and } E\left[\left\|\frac{\partial u_n^*}{\partial \nu}\right\|_{L^2(0,\Lambda)}^2\right] \le C. \tag{4.7}$$

From Theorem 3.1,

$$\begin{aligned}
E\left[\|D_{\alpha_1} R(\zeta;\boldsymbol{\alpha})\|_2^2\right] &\le C\max_{n\in\mathcal{N}} E\left[\|\hat{u}_n(\zeta;b)+\int_0^\Lambda\left(\frac{\partial \bar{u}}{\partial \nu}\cdot\frac{\partial u_n^*}{\partial \nu}\nu_2\right)\cdot D_{\alpha_1} f_1 dx_1\|_2^2\right]\\
&\le C\max_{n\in\mathcal{N}}\left[E\left[|\hat{u}_n(\zeta;b)|^2\right]+E\left[\|\int_0^\Lambda\left(\frac{\partial \bar{u}}{\partial \nu}\frac{\partial u_n^*}{\partial \nu}\nu_2\right)\cdot D_{\alpha_1} f_1 dx_1\|_2^2\right]\right].
\end{aligned}$$

Using (4.5)-(4.7) and the Cauchy-Schwartz inequality, we obtain

$$E\left[\|D_{\alpha_1} R(\zeta;\boldsymbol{\alpha})\|_2^2\right] \le C.$$

Similarly, we have

$$E\left[\|D_{\alpha_j} R(\zeta;\boldsymbol{\alpha})\|_2^2\right] \le C,\ j=2,\cdots,\ell.$$

Following the same lines, it can also be shown that

$$\|D_{\boldsymbol{\alpha}}^2 Q(\boldsymbol{\alpha})\|_2^2 = E\left[\|D_{\boldsymbol{\alpha}}^2 R(\boldsymbol{\alpha})\|_2^2\right] \le C. \tag{4.8}$$

Here $D_{\boldsymbol{\alpha}}^2$ denotes the Hessian matrix of $Q(\boldsymbol{\alpha})$.

Without loss of generality, we assume that $M_0 = 1$ in Algorithm 1, and the iteration becomes $\boldsymbol{\alpha}^{(n+1)} = \boldsymbol{\alpha}^{(n)} - h_n \cdot D_{\boldsymbol{\alpha}} R(\zeta; \boldsymbol{\alpha}^{(n)})$. Now, there exists $\widetilde{\boldsymbol{\alpha}} \in (\boldsymbol{\alpha}^{(n)}, \boldsymbol{\alpha}^{(n+1)})$ such that

$$\begin{aligned} & Q(\boldsymbol{\alpha}^{(n+1)}) - Q(\boldsymbol{\alpha}^{(n)}) \\ \leq & D_{\boldsymbol{\alpha}} Q(\boldsymbol{\alpha}^{(n)})^T (\boldsymbol{\alpha}^{(n+1)} - \boldsymbol{\alpha}^{(n)}) + \frac{1}{2} \| D^2_{\boldsymbol{\alpha}} Q(\widetilde{\boldsymbol{\alpha}}) \|_2^2 \cdot \| \boldsymbol{\alpha}^{(n+1)} - \boldsymbol{\alpha}^{(n)} \|_2^2 \\ \leq & D_{\boldsymbol{\alpha}} Q(\boldsymbol{\alpha}^{(n)})^T (\boldsymbol{\alpha}^{(n+1)} - \boldsymbol{\alpha}^{(n)}) + \frac{1}{2} C \| \boldsymbol{\alpha}^{(n+1)} - \boldsymbol{\alpha}^{(n)} \|_2^2 \\ = & -h_n D_{\boldsymbol{\alpha}} Q(\boldsymbol{\alpha}^{(n)})^T D_{\boldsymbol{\alpha}} R(\zeta_n; \boldsymbol{\alpha}^{(n)}) + \frac{1}{2} h_n^2 C \| D_{\boldsymbol{\alpha}} R(\zeta_n; \boldsymbol{\alpha}^{(n)}) \|_2^2. \end{aligned} \tag{4.9}$$

Let us take conditional expectation of (4.9) with respect to ζ_n. Then $E_{\zeta_n}[\| D_{\boldsymbol{\alpha}} R(\zeta_n; \boldsymbol{\alpha}^{(n)}) \|_2^2 \leq C$ since $E[\| D_{\boldsymbol{\alpha}} R(\zeta_n; \boldsymbol{\alpha}^{(n)}) \|_2^2 \leq C$. It follows that

$$\begin{aligned} E_{\zeta_n}[Q(\boldsymbol{\alpha}^{(n+1)})] - Q(\boldsymbol{\alpha}^{(n)}) & \leq -h_n D_{\boldsymbol{\alpha}} Q(\boldsymbol{\alpha}^{(n)})^T E_{\zeta_n}[D_{\boldsymbol{\alpha}} R(\zeta_n; \boldsymbol{\alpha}^{(n)})] + \frac{1}{2} h_n^2 C^2 \\ & \leq -h_n \| D_{\boldsymbol{\alpha}} Q(\boldsymbol{\alpha}^{(n)}) \|_2^2 + \frac{1}{2} h_n^2 C^2. \end{aligned}$$

Taking the expectation yields

$$E[Q(\boldsymbol{\alpha}^{(n+1)})] - E[Q(\boldsymbol{\alpha}^{(n)})] \leq -h_n E[\| D_{\boldsymbol{\alpha}} Q(\boldsymbol{\alpha}^{(n)}) \|_2^2] + \frac{1}{2} h_n^2 C^2. \tag{4.10}$$

Denote $Q_\infty := \liminf_{n \to \infty} Q(\boldsymbol{\alpha}^{(n)})$, then $Q_\infty > 0$. By adding (4.10) from 1 to n, we obtain

$$Q_\infty - E[Q(\boldsymbol{\alpha}^{(1)})] \leq E[Q(\boldsymbol{\alpha}^{(n+1)})] - E[Q(\boldsymbol{\alpha}^{(1)}] \leq -\sum_{j=1}^{n} h_j E[\| D_{\boldsymbol{\alpha}} Q(\boldsymbol{\alpha}^{(j)}) \|_2^2] + \frac{1}{2} C^2 \sum_{j=1}^{n} h_j^2.$$

Hence,

$$\sum_{j=1}^{n} h_j E[\| D_{\boldsymbol{\alpha}} Q(\boldsymbol{\alpha}^{(n)}) \|_2^2] \leq E[Q(\boldsymbol{\alpha}^{(1)})] - Q_\infty + \frac{1}{2} C^2 \sum_{j=1}^{n} h_j^2.$$

Since $\sum_{n=1}^{\infty} h_n^2 < \infty$, there holds

$$\lim_{n \to \infty} \sum_{j=1}^{n} h_j E[\| D_{\boldsymbol{\alpha}} Q(\boldsymbol{\alpha}^{(j)}) \|_2^2] < \infty. \tag{4.11}$$

On the other hand, since $U_{\boldsymbol{\alpha}}$ is closed, it follows that

$$\begin{aligned} E[\| D_{\boldsymbol{\alpha}} Q(\boldsymbol{\alpha}^{(n+1)}) \|_2^2] - E[\| D_{\boldsymbol{\alpha}} Q(\boldsymbol{\alpha}^{(n)}) \|_2^2] & \leq \max_{\boldsymbol{\alpha} \in U_\alpha} \| D^2_{\boldsymbol{\alpha}} Q \|_2^2 \cdot E[\boldsymbol{\alpha}^{(n+1)} - \boldsymbol{\alpha}^{(n)}] \\ & \leq h_n \max_{\boldsymbol{\alpha} \in U_\alpha} \| D^2_{\boldsymbol{\alpha}} Q \|_2^2 \cdot E[D_\alpha R(\zeta_n, \boldsymbol{\alpha}^{(n)})] \\ & \leq C^2 h_n. \end{aligned} \tag{4.12}$$

From (4.11),(4.12) and Lemma 4.2, we deduce that $E\left[\| D_{\boldsymbol{\alpha}} Q(\boldsymbol{\alpha}^{(n)}) \|_2^2\right] \to 0$ as $n \to \infty$.

5 Numerical experiments

In this section, we present several numerical examples to demonstrate the efficiency of the numerical algorithm for solving the optimal design problems. The first numerical example tests the efficiency of the stochastic gradient descent method for solving the optimization problem and its performance compared to the full gradient descent method. In the second example, we apply Algorithm 1 to solve the optimization problem (I) at fixed frequency. Example 3 and Example 4 demonstrate the efficiency of Algorithm 1 when it is applied to the optimization problem (II) and (III) in the case of broad-band frequency and multiple incident angles. In all examples, we set the sample size $M_0 = 5$ and use $\tilde{R} := \frac{1}{M_0} \sum_{m=1}^{M_0} R(\zeta_m; \boldsymbol{\alpha}^{(n)})$ and $\|\tilde{G}\| := \frac{1}{M_0} \| \sum_{m=1}^{M_0} D_{\boldsymbol{\alpha}} R(\zeta_m; \boldsymbol{\alpha}^{(n)}) \|_2$ to denote the average reflectivity and the average amplitude of the gradient at each iteration. For all examples, the average thickness of the each layer is set as 300 nm, and the size of the periodic cell $\Lambda = 1500$ nm. The state and adjoint problems are solved by the finite element method, where for each random realization of the optical structure, each subdomain D_j is discretized by a triangular mesh such that the interface Γ_j shares the common side of two adjacent triangles located above and below Γ_j respectively.

Example 1 For simplicity we do not explicitly consider the glass substrate and assume that the solar cell consists of an absorbing layer (e.g., a-Si:H) at the bottom and a transparent conducting oxide (TCO) layer on the top. The bottom of the structure Γ_1, and the interface Γ_2 between the absorbing layer and the TCO layer are randomly texutured. Assume that the free space wavelength $\lambda_0 = 650$ nm. The relative permittivity of the TCO layer is $\varepsilon_{r,1} = 3.667$, and the relative permittivity for the absorbing layer is $\varepsilon_{r,2} = 17.6380 + 0.3780i$ [10, 13, 18]. We consider the configuration when the incident angle $\theta = 0$.

Assume that the interfaces Γ_1 and Γ_2 are random processes with the covariance function $c_j(x_1 - \tilde{x}_1) = \left(\alpha_j^{(1)}\right)^2 \exp\left(-|x_1 - \tilde{x}_1|^2 / \left(\alpha_j^{(2)}\right)^2\right)$. The initial guess is chosen to be $(\alpha_1, \alpha_2) = (35\text{nm}, 20\text{nm})$. We apply both the full gradient descent method (4.1) and the stochastic gradient descent method described in Algorithm 1 to solve the optimization problem (2.19), where the gradient $D_{\boldsymbol{\alpha}} R(\zeta_m; \cdot)$ is computed via formulas (3.1a) and (3.1b). The stopping criteria is set as the amplitude of the average gradient amplitude $\|\tilde{G}\|$ being less than 0.05.

Figure 3 shows the value of the average reflectivity $\tilde{R}$ at each iteration for the stochastic gradient method when the random variables in the Karhunen–Loève expansion (2.14) are chosen to be uniform and Gaussian random variables, respectively. For the former, the reflectivity $\tilde{R}$ decreases quickly in the first 50 iterations and it takes about 180 iterations to achieve the stopping criteria, while it only takes about 60 iterations for the latter to achieve the same tolerance. For completeness we also show the amplitude of the gradient $\|\tilde{G}\|$ at each iteration in Figure 4. It is clear that while $\|\tilde{G}\|$ oscillates during the

iterations but the envelope of $\|\tilde{G}\|$ decreases as n increases. This is consistent with our convergence analysis presented in Section 4.

Figure 5 shows the reflectivity Q for each iteration when the full gradient descent method is applied. Here the Monte Carlo method is used for sampling the random space. Table 1 and Table 2 collect the optimal parameters obtained by two different numerical approaches. It is observed that the optimal parameters obtained by the stochastic gradient descent method and the full gradient descent method are close to each other.

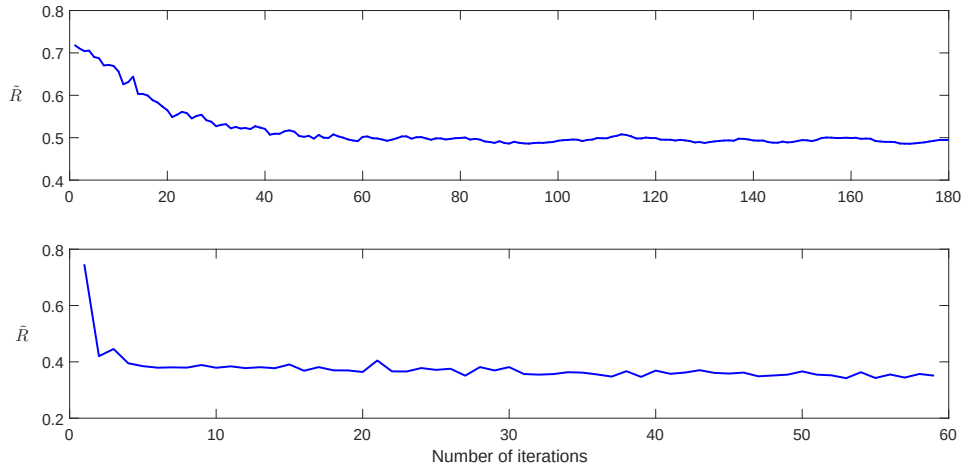

Figure 3: The reflectivity value $\tilde{R}(\boldsymbol{\alpha})$ during the stochastic gradient descent iterations. Top: $\{\xi_0, \xi_{m,s}, \xi_{m,c}\}$ are uniform random variables; Bottom: $\{\xi_0, \xi_{m,s}, \xi_{m,c}\}$ are Gaussian random variables.

Table 1: The optimal values of $\alpha^{(1)}$ and $\alpha^{(2)}$ obtained by the full gradient method and the stochastic gradient method for uniform random variables.

optimal result(nm)	$\alpha_1^{(1)}$	$\alpha_1^{(2)}$	$\alpha_2^{(1)}$	$\alpha_2^{(2)}$	reflectivity
Full gradient method	41	30	38	26	0.503
Stochastic gradient method	44	33	35	24	0.495

Though the optimal solutions obtained by the full gradient and the stochastic gradient methods are close, their computational cost is significantly different. When the Monte Carlo method is applied to sample the probability space, the sample size needs to be large. In our numerical experiment, the sample size is chosen to be 1000 for each iteration. When the optical wavelength is 650nm, the computation of the gradient $D_{\boldsymbol{\alpha}} R(\zeta, \boldsymbol{\alpha})$ for each sample ζ requires solving the boundary value problem (2.13) once and 9 adjoint problems (3.2) with all propagating modes. The full gradient algorithm stops after 7 steps, thus it requires solving 70000 boundary value problems. On the other hand, the 60 stochastic gradient descent iterations only requires solving no more than 3000 boundary

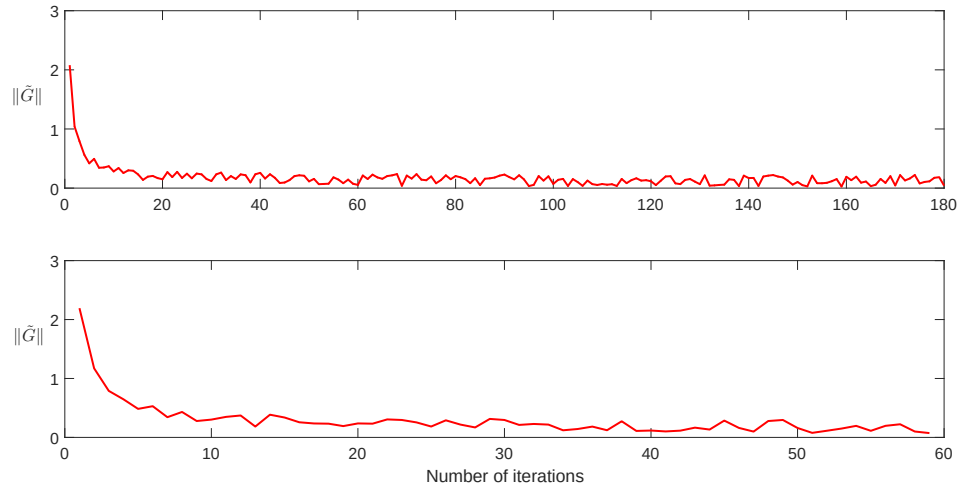

Figure 4: The amplitude of the average gradient $\|\tilde{G}\|$ during the stochastic gradient descent iterations. Top: $\{\xi_0,\xi_{m,s},\xi_{m,c}\}$ are uniform random variables; Bottom: $\{\xi_0,\xi_{m,s},\xi_{m,c}\}$ are Gaussian random variables.

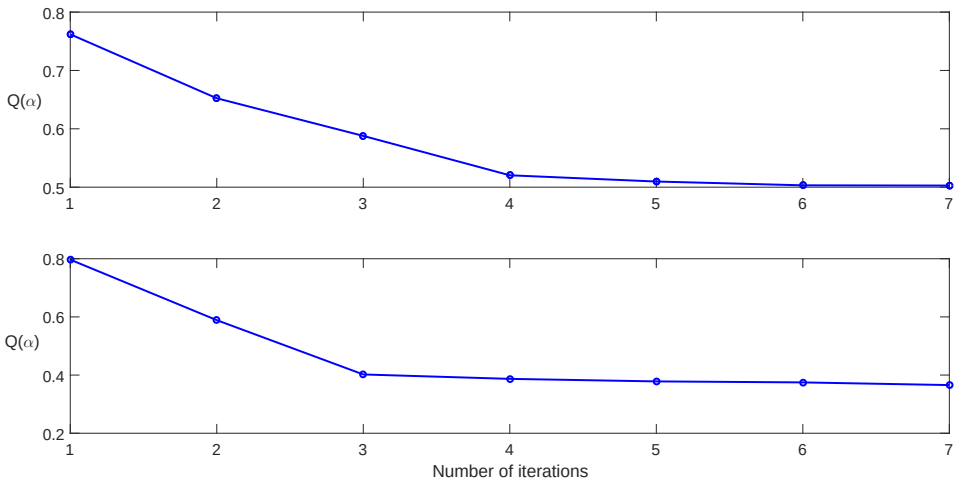

Figure 5: The reflectivity value $Q(\boldsymbol{\alpha})$ during the full gradient iterations. Top: $\{\xi_0,\xi_{m,s},\xi_{m,c}\}$ are uniform random variables; Bottom: $\{\xi_0,\xi_{m,s},\xi_{m,c}\}$ are Gaussian random variables.

Table 2: The optimal values of $\alpha^{(1)}$ and $\alpha^{(2)}$ obtained by the full gradient method and the stochastic gradient method for Gaussian random variables.

optimal result(nm)	$\alpha_1^{(1)}$	$\alpha_1^{(2)}$	$\alpha_2^{(1)}$	$\alpha_2^{(2)}$	reflectivity
Full gradient method	55	67	40	17	0.364
Stochastic gradient method	57	63	42	15	0.352

value problems. Therefore, the stochastic gradient descent method lowers the computational cost dramatically.

Example 2 Consider the multiple-layer solar cell structure as shown in Figure 6, where the interfaces of the two TCO layers are patterened randomly. The refractive index of the TCO, the absorbing layer and the glass substrate are 1.915, $4.2+0.045i$ and 1.4, respectively. Let the incident angle $\theta = 0$ and the wavelength $\lambda_0 = 650$ nm. We assume that all the interfaces are Gaussian random processes.

It takes about 120 iterations for the stochastic gradient descent method to achieve the desired tolerance, and the average reflectivity $\tilde{R}$ for each iteration is shown in Figure 7. The reflectivity $\tilde{R}$ decreases from the initial value 0.75 to 0.37 for the optimal random structure, with the corresponding absorptance value 0.63. As a comparison, the absorptance of the structure with all flat interfaces is only 0.13. Figure 8 depicts the wave field for one realization of random structure with the optimal result and Figure 9 shows the wave field for the structure with flat interfaces. It is observed that the waves are scattered in the random medium, which elongates the optical path and increases the overall absorptance of the structure.

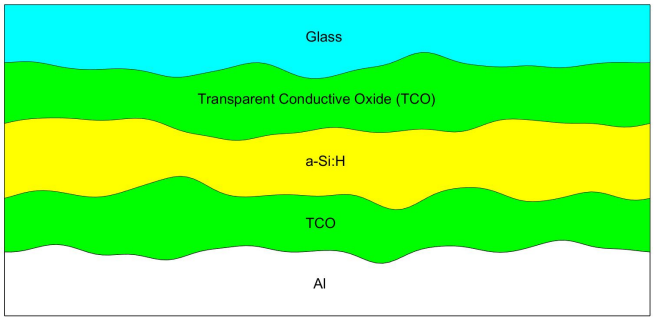

Figure 6: Optical structure with four random interfaces.

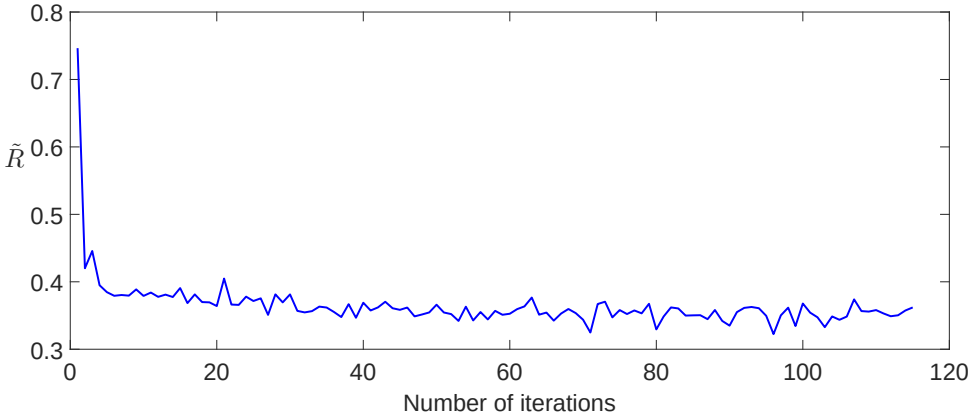

Figure 7: The reflectivity value $\tilde{R}(\boldsymbol{\alpha})$ during the stochastic gradient iterations for Problem(I). The multi-layered medium has four random interfaces shown in Figure 6.

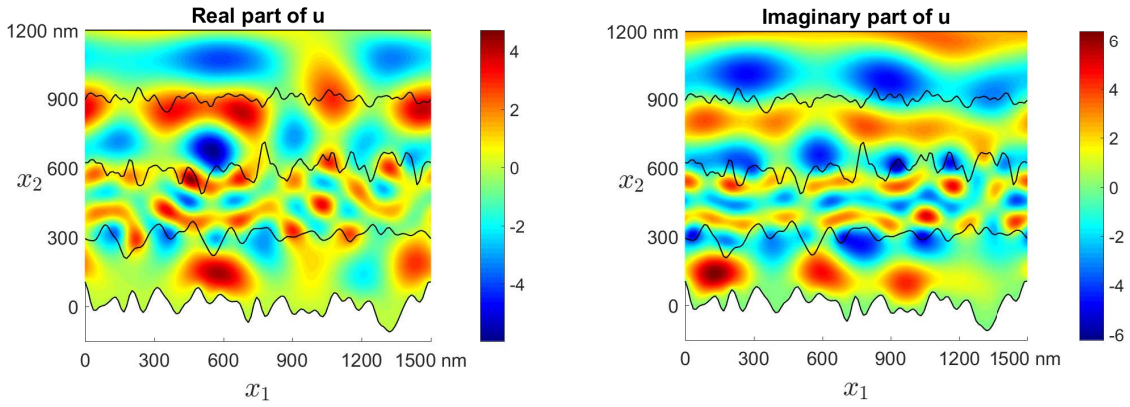

Figure 8: Numerical solution of the boundary value problem (2.13) for one realization of random structure with optimal parameters.

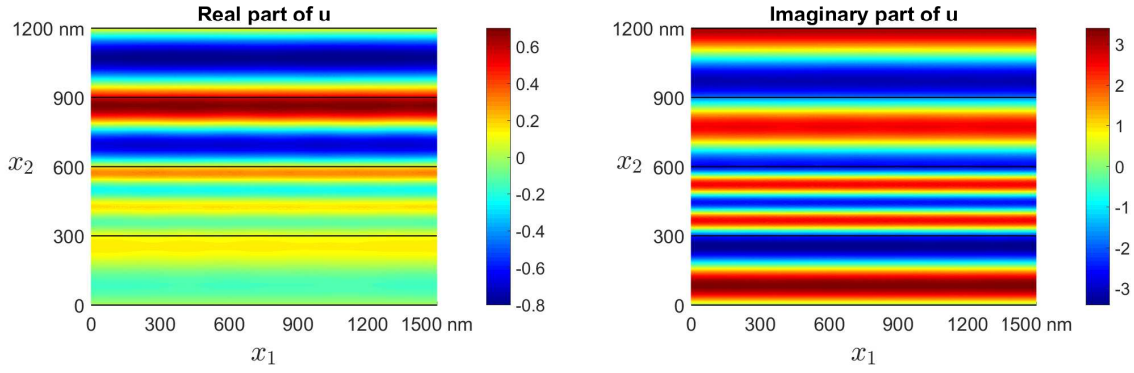

Figure 9: Numerical solution of the boundary value problem (2.13) when all the interfaces are flat.

Example 3 In this example, we consider the more challenging optimization problem with multiple frequencies, which is formulated in (2.20). Let us still use the multi-layer structure shown in Figure 6. Assume that the interfaces are Gaussian random processes and the incident angle $\theta=0$. The refractive index of the absorbing layer is set as $4.5+0.12i$ and $4.2+0.045i$ when $\lambda_{min}=600$ nm and $\lambda_{max}=650$ nm, respectively. For simplicity, we assume the refractive index of the absorbing layer is a linear function of the wavelength between λ_{min} and λ_{max}.

The integral $\int_{\lambda_{min}}^{\lambda_{max}} R(\zeta;\boldsymbol{\alpha},\lambda)d\lambda$ in (2.20) is approximated by the sum $\frac{1}{M_\lambda}\sum_{m=1}^{M_\lambda} R(\zeta;\boldsymbol{\alpha},\lambda_m)$, in which $\lambda_m=\lambda_{min}+\frac{\lambda_{max}-\lambda_{min}}{M_\lambda-1}(m-1)$ for $m=1,\cdots,M_\lambda$. We consider the normal incidence with the incident angle $\theta=0$.

Figure 10 shows the average reflectivity at each iteration for the stochastic gradient descent approach. It is calculated the average reflectivity of the optimal structure is about 0.28 and the average absorptance is about 0.72. We see that the absorptance is significantly enhanced compared to the structure with flat interfaces, which only attains the value 0.24.

Example 4 In this example, we consider the optimization problem with multiple incident angle for the structure shown in Figure 6. The problem is formulated in (2.21). We still consider the interfaces with Gaussian random processes and solve the problem with the stochastic gradient descent method. In the calculation, the integral $\int_{\theta_{min}}^{\theta_{max}} R(\zeta;\boldsymbol{\alpha},\theta)d\lambda$ is approximated with the sum $\frac{1}{M_\theta}\sum_{m=1}^{M_\theta} R(\zeta;\boldsymbol{\alpha},\theta_m)$, where $\theta_m=\theta_{min}+\frac{\theta_{max}-\theta_{min}}{M_\theta-1}(m-1)$ for

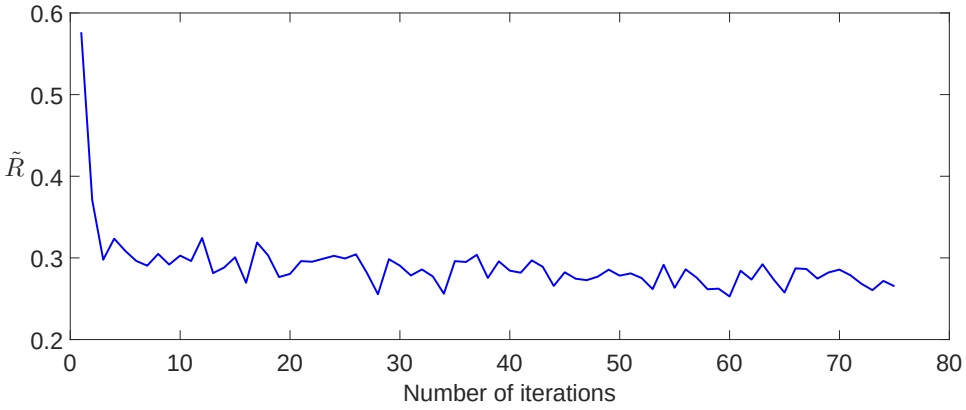

Figure 10: The reflectivity value $\tilde{R}(\boldsymbol{\alpha})$ during the stochastic gradient iterations for Problem (II).

$m=1,\cdots,M_\theta$. When the range of the incident angle starts from $\theta_{min}=-\frac{\pi}{12}$ to $\theta_{max}=\frac{\pi}{12}$, the reflectivity at each stochastic gradient iteration is shown in Figure 11. We obtain an average absorptance value of about 0.51 for the optimal structure, which again is significantly higher than the the structure with flat interface with an absorptance value 0.11.

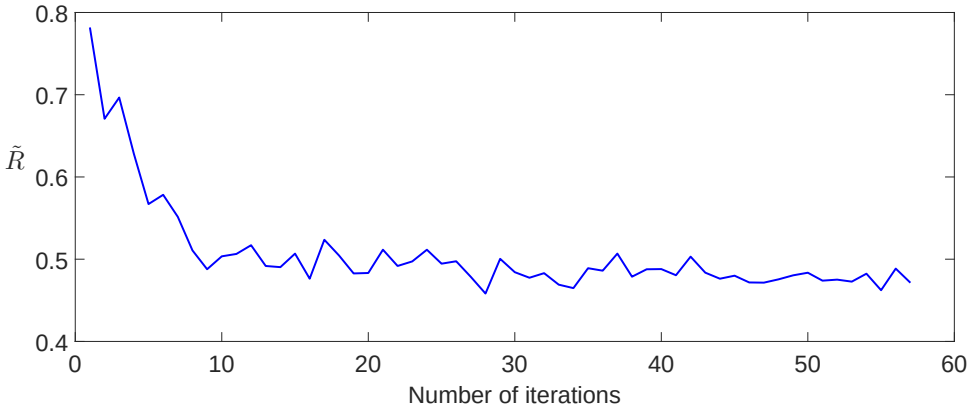

Figure 11: The reflectivity value $\tilde{R}(\boldsymbol{\alpha})$ during the stochastic gradient iterations for Problem (III).

Acknowledgments

The work of YC was partially supported by the DOE grant DE-SC0022253, and the work of JL was partially supported by the NSF grant DMS-1719851 and DMS-2011148.

References

[1] C. Battaglia, *et al.*, *Light trapping in solar cells: can periodic beat random?*, ACS Nano, **6** (2012): 2790-2797.

[2] G. Bao, D. Dobson, and J. Cox, *Mathematical studies in rigorous grating theory*. J. Opt. Soc. Amer. A, **12** (1995), 1029-1042.

[3] G. Bao and Y. Wang, *Optimal design of antireflection coatings with different metrics*, J. Opt. Soc. Am. A, **30** (2013), 656-662.

[4] G. Bao, Y. Cao, J. Lin and H. W. Van Wyk, *Computational optimal design of random rough surfaces in thin-film solar cells*, Commun. Comput. Phys., **88** (2019), 1815-2406.

[5] G. Bao and J. Lin, *Imaging of local surface displacement on an infinite ground plane: the multiple frequency case*, SIAM J. Appl. Math., **71** (2011), 1733-1752.

[6] P. Bermel, C. Luo, L. Zeng, L. Kimerling, and J. Joannopoulos, *Improving thin-film crystalline silicon solar cell efficiencies with photonic crystals*, Opt. Express **15** (2007), 16986.

[7] L. Bottou and F. E. Curtis and J. Nocedal, *Optimization methods for large-scale machine learning*, SIAM Rev., **60** (2018), 223-311.

[8] A. Bonnet-Bendhia and F. Starling, *Guided waves by electromagnetic gratings and non-uniqueness examples for the diffraction problem*, Math. Meth. Appl. Sci., **17** (1994), 305-338.

[9] A. Čampa, J. Krč, and M. Topič, *Analysis and optimisation of microcrystalline silicon solar cells with periodic sinusoidal textured interfaces by two-dimensional optical simulations*, J. Appl. Phys., **105** (2009), 083107.

[10] S. Fahr, C. Rockstuhl, and F. Lederer, *Engineering the randomness for enhanced absorption in solar cells*, Appl. Phy. Lett. **92** (2008): 171114.

[11] V. Ferry, M. Verschuuren, M. Lare, R. Schropp, H. Atwater and A. Polman, Optimized spatial correlations for broadband light trapping nanopatterns in high efficiency ultrathin film a-Si: H solar cells, Nano Lett. **11** (2011), 4239-4245.

[12] J. C. Goldschmidt *et al.*, *Increasing the efficiency of fluorescent concentrator systems*, Sol. Energy Mat. Sol. Cells, **93** (2009), 176-182.

[13] P. Kowalczewski, M. Liscidini, and L. Andreani, *Engineering Gaussian disorder at rough interfaces for light trapping in thin-film solar cells*, Opt. Lett., **37** (2012), 4868-4870.

[14] G. Lord, C. Powell, and T. Shardlow, *An Introduction to Computational Stochastic PDEs*, Cambridge University Press, 2014.

[15] X. Li and F. Orabona, *On the convergence of stochastic gradient descent with adaptive stepsizes*, The 22nd International Conference on Artificial Intelligence and Statistics, (2019), 983-992.

[16] S. Nicolay, M. Despeisse, F-J. Haug, and C. Ballif, *Control of LPCVD ZnO growth modes for improved light trapping in thin film silicon solar cells*, Solar Energy Materials and Solar Cells, **95** (2011), 1031-1034.

[17] J. A. Ogilvy, *Theory of wave scattering from random rough surfaces*, Adam Hilger, 1991.

[18] C. Rockstuhl, S. Fahr, K. Bittkau, T. Beckers, R. Carius, F-J. Haug, Thomas Söderström, Christophe Ballif, and F. Lederer, *Comparison and optimization of randomly textured surfaces in thin-film solar cells*, Opt. Exp., **18** (2010), A335-A341.

[19] C. Rockstuhl and F. Lederer, *Photon management by metallic nanodiscs in thin film solar cells*, Appl. Phys. Lett., **94** (2009), 213102.

[20] H. Robbins and S. Monro, *A stochastic approximation method the annals of mathematical statistics*, **22** (1951), 400-407.

[21] J. Sokolowski and J. P. Zolesio, *Introduction to Shape Optimization*, Springer Berlin Heidelberg, 1992.

[22] M. Zeman, R. Van Swaaij, J. Metselaar, and R. Schropp, *Optical modeling of a-Si:H solar cells with rough interfaces: Effect of back contact and interface roughness*, J. Appl. Phys., **88** (2000), 6436-6443.